R. & M. No. 3424

MINISTRY OF AVIATION

AERONAUTICAL RESEARCH COUNCIL
REPORTS AND MEMORANDA

Low-Speed Wind-Tunnel Experiments on a Series of Sharp-Edged Delta Wings

By P. B. EARNSHAW and J. A. LAWFORD

LONDON: HER MAJESTY'S STATIONERY OFFICE

1966

PRICE 18s. 0d. NET

Low-Speed Wind-Tunnel Experiments on a Series of Sharp-Edged Delta Wings

By P. B. Earnshaw and J. A. Lawford

Summary.

A series of six delta wings of varying angles of sweepback has been tested. A three-component strain-gauge balance was used to investigate the forces and moments, and normal-force fluctuations for incidences between ± 60°. Positions of vortex breakdown on these wings were noted. Surface flow pattern and boundary-layer transition observations were made.

The three most highly swept wings (*i.e.* having sweepback angles of 65°, 70° and 76°) appeared to have the most favourable characteristics of growth of normal-force fluctuations and had a smooth variation of forces and moments throughout the incidence range between positive and negative stalls.

The change from a vortex type of flow to one with complete flow reversal on the upper surface occurred at increased incidence with increase of sweepback angle. At moderate incidence α the main features of the flow pattern correspond to conical flow development, and correlate well with the single parameter $\alpha/\cot \phi$, where ϕ is the sweepback angle of the leading edge.

LIST OF CONTENTS

LIST OF ILLUSTRATIONS

---

1. *Introduction.*

This report describes an investigation of some features of the separated flow around sharp-edged delta wings of various leading-edge sweepback angles. It was early established that the separated flow from wings of zero or small sweepback takes the form of a closed 'bubble', whereas the highly swept wing sheds tightly rolled vortices. Tests were therefore planned to investigate the behaviour of the flow for a range of intermediate sweepback angles using a family of delta wings having leading-edge sweepback angles from 45° to 76°. A plano-convex section was used for ease of manufacture; it was thought that the effects of camber thus introduced would be comparatively small.

Results of three-component force measurements, normal-force fluctuation measurements, and surface flow visualisation are given, together with an assessment of the position of the breakdown of the vortex core within the incidence range during which it occurs forward of the trailing edge.

2. *Apparatus and Tests.*

A family of six cambered delta wings, having sharp leading edges with different angles of sweepback, were tested in the R.A.E. 4 ft × 3 ft Low Turbulence Wind Tunnel. Each wing had a 6% thick plano-convex chordwise section, the convex surface being generated by straight lines, drawn from the tips to the circular-arc centre-line section, giving geometrically similar chordwise

3

sections at all spanwise positions on all wings. The leading-edge sweepback angles were 76°, 70°, 65°, 60°, 55° and 45°. All the wings had a planform area of 0·347 sq.ft, with centre-line chords ranging from 0·589 ft to 1·178 ft. The models were of polished metal, and boundary-layer transition was not fixed.

Lift, drag and pitching-moment components were measured between incidences of ± 60° on two strain-gauge balances, one having a straight sting and the other having a sting cranked at 30° to the centre line of the balance. The former balance was used for wing incidences up to 30° and the latter for incidences between 25° and 60°. The balances were clamped and pivoted between two vertical, sliding struts (Fig. 1), which made it possible to position the models centrally in the tunnel at each incidence. The technique used was to clamp the model at a given incidence and to take balance readings with wind off before and after each reading with wind on. In order to explore the magnitude of the sting interference, forces were measured between ± 30° incidence by mounting the models on the straight sting with the flat and convex surfaces uppermost in turn, covering a full incidence range in both cases.

Normal-force fluctuations were measured using the strain-gauge balance system shown in Fig. 2. For this purpose the axial force balance of the three-component tests, turned through a right angle, was used as a normal-force balance because of its greater stiffness. The fluctuating signal from the balance was recorded on magnetic tape on an Ampex recorder, and the recordings were replayed and analysed using a Muirhead Pametrada Wave Analyser. The tests were made on the delta wing series at incidences from 0 to about 50°, again both with the convex surface and the flat surface uppermost. Normal-force fluctuations at positive incidence only were measured also on a 70° swept flat-plate delta wing, simply chamfered on one surface only to give sharp leading edges (Fig. 10), and on a rectangular wing of the same section as the plano-convex deltas; the unchamfered and convex surfaces respectively were defined as the upper surface. These two wings had the same planform area as those of the main series.

The position at which the tightly rolled leading-edge vortex breaks down to form a much more diffuse vortex was found by using a fine tuft, at the end of a rod inserted through the tunnel wall. At leading-edge sweep angles of 65°, 70° and 76°, the vortex core could be easily identified and the breakdown point clearly established. At the lower sweepback angles, the vortex core was less steady and the breakdown point could not be so clearly identified by this technique. At 45° sweepback, it could not be found at all, and it seems likely that the point of breakdown was very close to the apex of the wing. These vortex breakdown measurements were made using a wind speed of 80 ft/sec, but a few tests on the 65° delta with the wind speed increased to 160 ft/sec showed no change in breakdown point.

Surface flow tests were made using a support system similar to that used for the force measurements, but omitting the balance. Patterns were obtained using a mixture of paraffin oil and lampblack with a few drops of oleic acid as an anti-coagulant. The mixture was approximately three parts of oil to one of lampblack by volume, but thicker or thinner mixtures were frequently used, depending on the nature of the flow pattern; thicker mixtures were necessary for conditions giving high surface velocities, and *vice versa*.

Photographs were taken of the patterns formed on each model at incidences from 0 to 60° both with the convex and the flat surfaces uppermost. On the upper, or suction, surface observations were made at intervals of 5° in incidence, but on the lower surface larger intervals were used at the higher incidences.

4

In some cases an excessive amount of oil collected on a small area of the wing, giving a very dense and ill-defined pattern. This was cleaned off locally, a thin coat of the mixture was applied, and the tunnel was run again. The 'patch' effect in Figs. 15, 19, 21, 22, 23, 25 and 35 is due to this.

Tests were also made to determine the state of the boundary layer on the models over the same incidence range using the china-clay technique[5]. The models were sprayed first with black cellulose and then with china clay in a solution of nitro-cellulose ('dope'), so that when dry the surface appeared white, but when wetted with oil the china clay became transparent and the black underlayer showed through. Diesel oil of a suitable distillation fraction was used to moisten the surface, and Plasticene protuberances were used on the surface as required to help in the interpretation of the resulting patterns.

The wind speeds and corresponding Reynolds numbers (based on aerodynamic mean chord $\bar{c}$) for the tests were as follows:

Three-component balance tests	100 ft/sec ($0 \cdot 25 \times 10^6$ to $0 \cdot 50 \times 10^6$)
Normal-force fluctuation tests	80 ft/sec ($0 \cdot 20 \times 10^6$ to $0 \cdot 40 \times 10^6$)
Vortex breakdown tests	80 ft/sec ($0 \cdot 20 \times 10^6$ to $0 \cdot 40 \times 10^6$)
Surface flow visualisation	180 ft/sec ($0 \cdot 45 \times 10^6$ to $0 \cdot 90 \times 10^6$)

3. *Discussion of Results.*

3.1. *Forces and Moments.*

The normal force, lift, drag and pitching-moment characteristics of the six cambered delta wings are plotted in Figs. 3, 4, 5, 6 where positive incidences are defined as those incidences which have the plane surface on the pressure side. Experimental points for the two methods of mounting the models are not distinguished but are plotted generally in pairs at a particular incidence in these figures and illustrate the large sting interference effects which must exist, particularly in the case of pitching moments. However, irregularities on the curves could be reproduced by both methods, suggesting that the slopes of the curves can be drawn to a better accuracy than the scatter of the points implies.

Figs. 3, 4 show that the highest three sweepbacks provide smooth normal-force and lift curves between positive and negative stalls, whereas those for the lowest three sweepbacks are irregular at positive incidences, the 60° wing having a smooth curve up to 14° incidence where a 'kink' begins. All the wings have zero lift at the same incidence and, after the stall, all the families of curves shown in Figs. 3, 4. 5, 6 appear to approach common curves.

The normal-force curve for the 76° wing has a curious 'bucket' at the positive incidence stall, which was repeated at a wind speed of 140 ft/sec. In order to see whether this might indicate hysteresis, the method of test was altered and the incidence change made while the tunnel was running. The incidence was increased slowly to a point above and reduced to a point below the stall, producing the broken-line curve, shown in Fig. 3, for both increasing and decreasing incidence. The accuracy of these results was much reduced owing to zero wander during the run but a sufficiently large number of readings were taken to be sure that the stall did develop as shown. The possibility of the two distinct curves being produced by hysteresis with respect to change of incidence is therefore excluded. As no changes were discovered within the range of speed permitted by the equipment, this problem remains unresolved.

5

An attempt was made to fit the low incidence points on the $C_L - \alpha$ curves to a common curve, as demonstrated by Peckham. It was found possible with the 76°, 70° and 65° wings to determine, for each, a point about which the curve was antisymmetrical over a range of approximately $\pm 20°$, presumably the point of zero leading-edge vortex strength. Using this point as the new origin, $(C_L - C_{L0})/\sqrt{(C_0/S)}$ was calculated for several incidences on each wing and plotted in Fig. 7 along with Peckham's three symmetrical thick wings (12% thickness/chord ratio) and two symmetrical thin wings (1% thickness/chord ratio). It was found that an insufficient negative incidence range had been covered, on Peckham's asymmetrical thin wings, to apply the technique used for the present series; however, a rough value was taken for the centre of symmetry for one of these wings and the points plotted in the figure. It can be seen that a mean curve, drawn through the points from the thin wings, would be below Peckham's curve which, presumably, is affected by the finite leading-edge vortex strength existing at zero incidence. The thick wing B of Ref. 1 lies well below the other points. This wing, however, has a much greater volume, relative to the plan-form area, than the other thick wings which lie quite close to the revised curve although consistently below it. The heavily cambered thick wings of the present series lie on a curve which is above the revised curve at low incidence and below it at high incidence.

3.2. Normal-Force Fluctuations.

The results of the normal-force fluctuation measurements are presented in terms of the following quantities:

$$n = \text{Frequency parameter} = \frac{f\bar{c}}{V}$$

C_N = The root-mean-square intensity of fluctuation of the normal-force coefficient C_N.

$F(n)$ = The spectrum function, such that $F(n)dn$ is the contribution to $(C_N)^2$ of frequencies from n to $n + dn$,

i.e.

$$(C_N)^2 = \int_0^\infty F(n)dn .$$

The results are relevant to the problem of buffeting, which usually takes the form of excitation of a particular mode of structural vibration corresponding to a discrete frequency. The mode can be excited by load fluctuations at or close to this frequency, so that the structure has a sharply tuned resonance curve, or a narrow acceptance band. Thus, following the argument of Ref. 2, if f is the structural frequency and Δf the acceptance bandwidth in such a case, $\Delta f/f$ being small, the relevant root-mean-square intensity of the excitation $\sqrt{(\Delta C_N^2)}$ is given approximately by

$$\Delta C_N^2 = nF(n)\frac{\Delta n}{n} ,$$

i.e.

$$\sqrt{(\Delta C_N^2)} = \sqrt{\{nF(n)\}} \sqrt{\frac{\Delta f}{f}} , \text{ since } \frac{\Delta n}{n} = \frac{\Delta f}{f} .$$

The ratio $\Delta f/f$ is determined by the aircraft structural characteristics and is independent of wind speed. Hence $\sqrt{(\Delta C_N^2)}$ is directly proportional to $\sqrt{\{nF(n)\}}$, which is therefore a suitable quantity for the presentation of the results. The quantity $\sqrt{\{nF(n)\}}$ has been obtained at a fixed value of the frequency parameter, n.

6

In these tests the aerodynamic excitation is inferred from the response of the complete model, so it is obviously necessary to confine all measurements to frequencies well below the lowest natural frequency of the rig. Although care was taken to make this natural frequency as high as possible, and a relatively low tunnel speed of 80 ft/sec was used, the highest value of n at which reliable measurements could be made was $0 \cdot 05$. This is lower than the value of $0 \cdot 2$ which has been used in measurements of pressure fluctuations[2], and is probably rather low for the representation of likely aircraft critical conditions. However, it is of the correct order of magnitude and since the excitation spectrum has been found to be very flat in the low-frequency range, the value of $\sqrt{\{nF(n)\}}$ at $n = 0 \cdot 05$ would be expected to give a good indication of the level of excitation at probable buffeting frequencies.

All the measurements of normal-force fluctuation in this report are of this 'low-frequency component', and the term 'normal-force fluctuation' is to be taken as referring to this component only.

The results of the normal-force fluctuation measurements are plotted against incidence in Fig. 8, and against normal-force coefficient in Fig. 9, where positive incidences and coefficients are defined with the curved surface considered as the upper surface. In Fig. 10 the normal-force fluctuations on the 70° swept delta wing of this series are compared with those on the 70° swept flat-plate delta wing, all incidences in this case being treated as positive, with the appropriate definition of upper and lower surfaces.

At low incidence the normal-force fluctuations are small and almost constant. This is followed by an increase in the level of fluctuation to a value between ten and twenty times that at low incidence. This rise suggests a change in the nature of the aerodynamic excitation, and tends to imply the onset of a form of unsteadiness which could not be tolerated in practice. There is a marked change in the form of the curves at a sweepback angle of about 65°, the lower sweepbacks giving a sharp rise in normal-force fluctuation when the normal force is approximately half its maximum value, i.e. at comparatively low incidence, whereas the more highly swept wings show a more gradual increase in fluctuations until the normal force approaches its maximum. It appears therefore that there is less likely to be a buffet problem with wings of high leading-edge sweepback. The sharp kinks in the curves for the 55° and 60° swept wings at incidences of about 12° and 15° respectively coincide with kinks in the curves of lift coefficient against incidence (Fig. 4). There is a similar but smaller kink in the curve for the 65° swept wing, in this case without a noticeable kink in the lift curve.

The normal-force fluctuation measured at zero lift is very small, being of the same order of magnitude as that which would be caused by the component at this frequency of the known tunnel incidence fluctuation.

The normal-force fluctuation measurements on the 70° swept plano-convex and flat-plate delta wings (Fig. 10) show that, in this case, the primary factor is the shape of the upper surface, convexity or flatness of the lower surface having little effect.

3.3. Vortex Breakdown.

The chordwise position of the vortex breakdown point, expressed in terms of the centre-line chord (Figs. 11 and 12), moves forward with increase of incidence and with decrease of sweepback angle as expected. The following table lists the approximate position of the breakdown point when the normal-force fluctuations reach a level of $[\sqrt{\{nF(n)\}}]_{n = 0 \cdot 05} = 0 \cdot 0025$, that is, close to the start of the rapid rise in normal-force fluctuation.

While there is some variation from wing to wing, it is clear that the trend is for the rapid rise of normal-force fluctuation to occur when the vortex breakdown is close to the trailing-edge. When vortex breakdown is near the mid-point of the centre-line chord, normal-force fluctuations are high on all the wings.

Sweepback	Positive incidence		Negative incidence	
	α	Breakdown position	α	Breakdown position
45°	12	—	13	—
55°	13	0·85	18	0·85
60°	15	0·7	21	0·8
65°	29	0·95	26½	1·1 approx.
70°	6	1·0	34	1·1 approx.
76°	35	1·1 approx.	37	0·85

The vortex breakdown point is farther aft at positive incidence than at the corresponding negative incidence (except in the region of 20° incidence at 65° sweepback). Since the lift coefficient is numerically greater at positive incidence than at the equivalent negative incidence, this applies to a greater extent at corresponding lift rather than incidence.

3.4. Surface-Flow Patterns.

The nature of the flow over sharp-edged delta wings at moderate incidence is now well known. Vortex sheets are shed off the leading edges, and blow back over the upper surface, rolling up to form a pair of stable vortices. This causes a strong outflow on the upper surface below the vortices, which separates from the surface before reaching the leading edge, at a secondary separation line. Between this line and the leading edge there is at least one smaller and weaker vortex, as sketched in Fig. 13. There can be more than one vortex in this secondary region, but the surface shear is very small and the associated surface flow pattern cannot easily be defined experimentally.

Patterns of this type were obtained on the suction surface of all the delta planforms tested. Examples on the 55° and 76° swept wings are shown in Figs. 14 and 15. The positions of the main vortex attachment line and of the secondary separation line varied with incidence and with planform. But, for moderate incidences with the flat surface uppermost, the positions of both lines were found to correlate well with the single parameter $\alpha/\cot\phi$, where ϕ is the angle of sweepback of the leading edge and α is incidence relative to the no-lift angle, which, in all cases, corresponded to a geometric incidence of the plane surface of 2°. This supports earlier observations by Marsden, Simpson and Rainbird[5]. It implies, as does the straightness of the observed attachment and secondary separation lines, that the flow is roughly conical in these conditions. The ratio of flat-upper-surface attachment position to local semispan for all the wings is plotted against $\alpha/\cot\phi$ in Fig. 16. Except for the 45° swept delta wing, on which the flow was probably never approximately conical, and above which a tightly rolled vortex may not be formed[1], the observations are fairly well represented by a single curve. The theoretical curve derived by Mangler and Smith[6] is also shown in Fig. 16; agreement with measured values is poor.

8

On all planforms there formed at some incidences a 'whorl' near the outboard tips (*see* Fig. 20) where the secondary separation line bent outwards and the main vortex outflow passed round it and forwards close to the leading edge. The flow which it is suggested gives rise to this surface flow pattern is sketched in Fig. 17, and further examples are shown in Figs. 18 and 19. The whorl pattern appeared at quite low incidence on all the wings. Except in the case of the 45° swept leading edge, increasing incidence at first led to its disappearance, but it subsequently reappeared and was always a feature of the transition from the 'vortex' type of surface flow pattern to the complete flow reversal associated with the bluff-body wake which occurred at very high incidence. On the 45° swept wing with curved surface uppermost the whorl pattern was present at all incidences from 5° up to the stall, and was the dominant feature of the pattern from 10° incidence upwards (Fig. 20). Following its second appearance on the other wings, increase of incidence caused the whorl to move forward near the leading edge, the region of forward curvature of the main vortex outflow becoming larger and a forward flow developing over the trailing edge (Figs. 21 and 22). This flow is obviously very complex. Fig. 23 shows a surface pattern on the 55° swept wing at 30° incidence, with the flat surface uppermost, on which there is an outflow from the centre line and a forward flow from the trailing edge, with apparently a separation line where the two flows meet. The surface shear near the apex is very weak. At still higher incidence the flow was predominantly forward from the trailing edge (Figs. 24 and 25), the apex flow remaining weak. Some patterns in this condition showed what appeared to be a secondary separation near the apex but, at high incidence with a weak forward flow, gravity effects might be significant and this apparent separation could have been spurious.

Fig. 26 shows how the type of surface flow pattern varied with incidence on each wing. All the wings behaved in a similar way with increase of incidence, change of pattern from one form to another taking place at higher incidence for higher sweepback angle. Incidences for maximum lift and maximum normal force are approximately equal on these wings (*see* Figs. 3 and 4) and this incidence, and that at which vortex breakdown occurred at the mid-chord point, are included on Fig. 26. At the lower sweepback angles, maximum lift occurred just before forward flow developed near the trailing edge, but at the higher sweepback angles leading-edge vortex flow continued over the whole surface beyond the maximum lift point, for approximately 12° of incidence in the case of the 76° swept wing. Vortex breakdown took place at the mid-chord position at an incidence approximately 10° to 15° lower than the lowest incidence for flow reversal on all the wings.

The surface flow on the lower surface was of the type shown in Figs. 27 and 28 at all incidences on all the wings, an attachment line moving inwards from near the leading edge with increase of incidence with separation at the leading and trailing edges.

3.5. *Boundary-Layer Transition Patterns.*

Diagrams showing the distribution of laminar and turbulent boundary layers as shown by the china-clay technique are given in Figs. 29 to 33, and a specimen transition pattern is shown in Fig. 34 for the 70° swept wing at 10° incidence with the flat surface uppermost. The wedge of turbulent flow behind the Plasticene protuberance inboard of the secondary separation line can be clearly seen, while there was no wedge from the one near the leading edge where the surface shear was evidently very weak. In this case there was a small region of turbulent flow near the centre at the trailing edge.

9

At zero incidence, the boundary layer on the flat surface was predominantly turbulent for all the wings tested, but there was a small laminar region near the apex (except in the case of 60° sweepback), and a region of laminar flow near the tips (except on the 76° swept wing). Fig. 26 indicates the probable cause of this pattern. At zero incidence, vortex separation occurred only over part of the span near the apex, and was followed by attached flow near the tips. This was evidently due to the inherent type of camber which caused some leading-edge separation at all incidences and precluded the smooth development of the leading-edge vortices at very low incidence. It seems clear, and has subsequently been confirmed in other experiments, that if the wings had been uncambered, or the camber designed to the leading-edge restrictions proposed by Maskell and Weber[7], the boundary layer would have been laminar everywhere when attachment occurred at the leading edge. In the present case, transition was caused by the very weak part-span vortices. Increase of incidence, with the flat surface uppermost, and the consequent strengthening of the leading-edge vortices along the entire span, established regions of laminar flow under the vortices and inboard of the secondary separation lines. At the lower sweepback angles there remained, however, a central region of turbulent flow which spread out over the entire span near the trailing edge. With further increase of incidence the laminar regions extended right back to the trailing edge and, except on the wings with 55° and 60° sweepback, the central turbulent region was reduced in size. Before the incidence for reversal of the surface flow was reached, the boundary layer again became turbulent everywhere, and remained so up to the highest incidence of the experiments.

On the curved surface, the flow was attached at zero incidence for all the wings, and the boundary layer was mainly laminar apart from local turbulence near the sting. As incidence was increased with the convex surface uppermost, the flow first became turbulent from the tips, behind that part of the leading edge where the vortex first developed (Fig. 26). At 10° incidence, the boundary layer was entirely turbulent on all the wings and for 55° and 60° leading-edge sweepback it remained so as incidence was further increased, apart from local laminar regions near the apex. But with the higher sweepback angles laminar flow again developed under the vortices, in some cases with transition to turbulence near the trailing edge. At still higher incidence the flow again became entirely turbulent.

The boundary layer on the lower surface, both flat and convex, was laminar at all incidences from 5° upwards.

Close comparison of corresponding transition and oil-flow patterns on the upper surface shows a dark region on the transition pattern just inboard of the secondary separation line, indicating small, laminar surface shear and, where it extends up to the separation line, laminar separation. But in some cases a distinctly whiter region was observed just outboard of this dark line, suggesting transition followed by turbulent separation. Two such patterns, and the corresponding oil-flow patterns, are given in Figs. 34 and 35. In some cases this transition before secondary separation was accompanied by striations in the laminar region inboard of the separation line (Fig. 34) suggesting the cause of transition to be instability of the kind discussed theoretically by Owen and Randall[8], and Stuart[9] and studied experimentally by among others, Gray[10] and Gregory and Walker[9].

3.6. *Some Features of the Surface Flow and Transitional Patterns.*

A feature of the oil-flow pattern on all the wings except the 45° swept wing was the appearance of a kink in the secondary separation line, so that the separation was closer to the leading edge

10

(in terms of local span) at the rear of the wing. The kink first appeared near the trailing edge as incidence was increased, and steadily moved towards the apex. This trend is similar to that of the breakdown position of the vortex core; the positions of vortex breakdown and of kinking in the secondary separation line are compared in Fig. 37. For moderate leading-edge sweepback angles, the kink and the vortex breakdown were at approximately the same chordwise position, the breakdown point being in general a little farther aft. At higher sweepback angles the kink occurred at incidences at which the vortex breakdown was well downstream, and under such conditions appeared to be associated with the transition from laminar to turbulent separation (Figs. 34, 35). It seems possible that a kink in the secondary separation line may be caused by either of these distinct features of the flow. Kinks due to these two causes appear to differ slightly in form, that due to turbulent separation (Fig. 35) being an outward displacement of the separation line, while that due to vortex breakdown is rather a decrease of sweepback of the separation line (Fig. 38).

An unexpected feature of the surface oil-flow patterns was the appearance of an apparent separation line near the trailing edge on the convex lower surface at small incidences with the flat surface uppermost. This appeared on all the wings at incidences from 0° to 10°, as illustrated in Fig. 39 for the 65° swept wing at 10° incidence, and is not fully understood. Although it may well have been a genuine laminar separation, it also seems possible that the oil was moving more under the influence of the pressure gradients than of the obviously weak laminar shear, and that the pattern is therefore spurious. When transition was forced by Plasticene protuberances farther forward this feature of the pattern was eliminated.

4. Conclusions.

The flow around the three most highly swept wings of this series leads to a smooth variation of forces and moments with incidence, between the positive and negative stalls. For the lower sweep angles, however, this variation is irregular at positive incidence when the curved surface is uppermost.

The low-frequency normal-force fluctuations rise sharply at comparatively low incidence (between 10° and 20°) for leading-edge sweepback angles of less than 65°. With greater sweepback, these fluctuations rise more slowly with increase of incidence; if the leading-edge sweepback is between 65° and 76°, there is no substantial rise until maximum normal force is approached.

At both constant incidence and constant lift, the vortex breakdown point is farther forward when the flat surface is uppermost than when the curved surface is uppermost. In most cases, the low-frequency normal-force fluctuations begin to increase rapidly with incidence when the vortex breakdown point moves forward of the trailing-edge.

The surface flow pattern on the upper surface changes with increase of incidence from that associated with vortex flow to one with complete flow reversal, the change occurring at higher incidence with increase of sweepback angle.

At moderate incidences, the main features of the flow pattern indicate roughly conical flow development and correlate well with the single parameter $\alpha|\cot\phi$, where ϕ is the leading-edge sweepback angle.

A sufficiently strong primary vortex tends to favour the maintenance of laminar flow in the boundary layer from some way inboard of its associated attachment line to the secondary separation line. At the rather low Reynolds numbers of the present experiments, the region of laminar flow

11

under such a vortex tends to increase in extent with increase of incidence and therefore of vortex strength. But very small vortices, probably partially or wholly immersed in the boundary layer, behave as boundary-layer trips, effectively promoting transition at the leading edge; at high incidence, though before flow reversal occurs, the boundary layer always becomes fully turbulent.

Evidence was found of transition from laminar to turbulent secondary separation due to boundary-layer instability of the Owen-Stuart type.

LIST OF REFERENCES

No.	Author(s)	Title, etc.
1	P. H. Peckham	Low-speed wind-tunnel tests on a series of uncambered slender pointed wings with sharp edges. A.R.C. R. & M. 3186. December, 1958.
2	T. B. Owen	Techniques of pressure-fluctuation measurements employed in the R.A.E. low-speed wind-tunnels. AGARD Report 172. March, 1958.
3	E. J. Richards and F. H. Burstall	The 'China clay' method of indicating transition. A.R.C. R. & M. 2126. August, 1945.
4	E. C. Maskell	Flow separation in three dimensions. R.A.E. Report Aero. 2565. A.R.C. 18 063. November, 1955.
5	D. J. Marsden, R. W. Simpson and W. J. Rainbird	An investigation into the flow over delta wings at low speeds with leading-edge separation. C.o.A. Report 114. A.R.C. 20 409. September, 1958.
6	K. W. Mangler and J. H. B. Smith	A theory of slender delta wings with leading-edge separation. *Proc. Roy. Soc.* A, Vol. 251, p. 200. May, 1959.
7	E. C. Maskell and J. Weber ..	On the aerodynamic design of slender wings. *J.R.Ae.S.*, Vol. 63, No. 588, pp. 709 to 721. December, 1959.
8	P. R. Owen amd P. G. Randall	Boundary layer transition on a sweptback wing. A.R.C. 15 022. May, 1952.
9	Gregory, Stuart and Walker ..	Boundary layer effects in aerodynamics. N.P.L. Symposium. H.M.S.O. 1955. Part 3. On the stability of three-dimensional boundary layers, with application to the flow due to a rotating disk.
10	W. E. Gray	The nature of the boundary layer flow at the nose of a swept wing. A.R.C. 15 021. June, 1952.
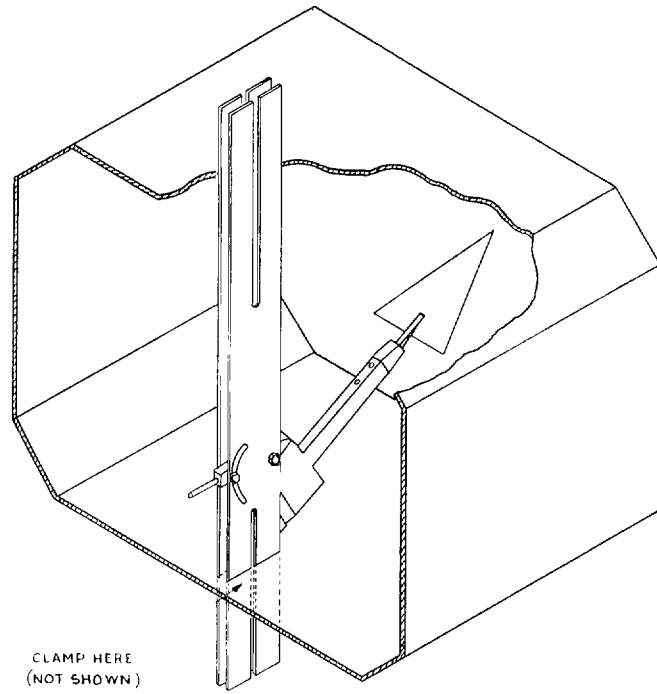
FIG. 1. General arrangement of model, balance, and supporting strut in the 4 ft × 3 ft Tunnel.
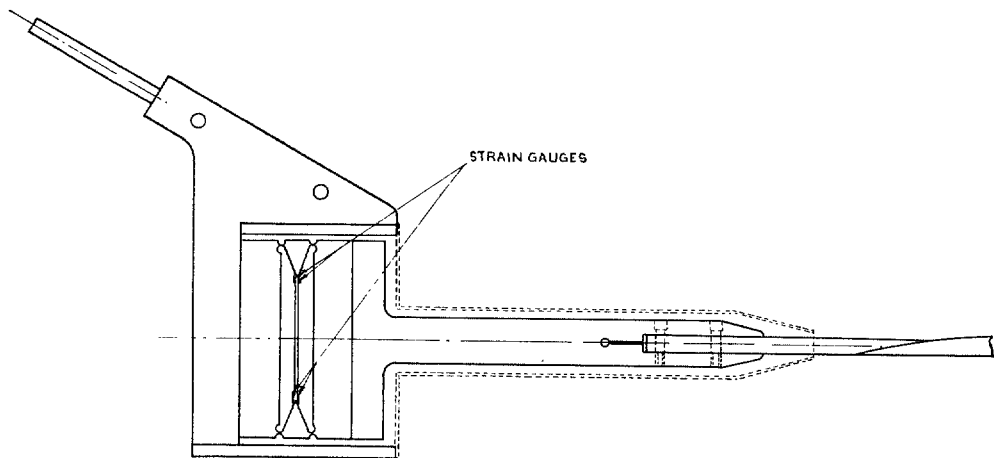
FIG. 2. General arrangement of strain-gauge balance for measurement of normal-force fluctuations.
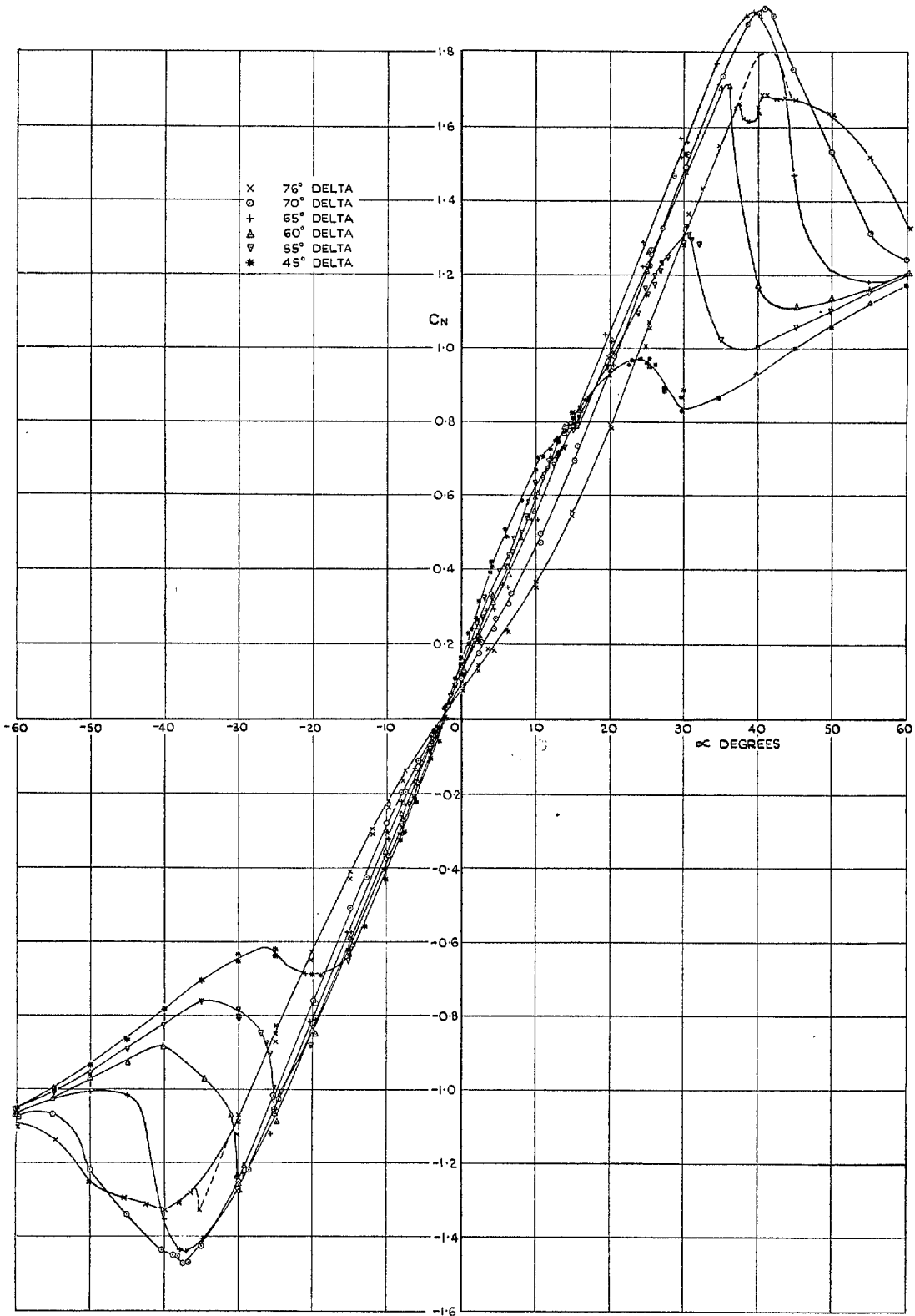
FIG. 3. Variation of normal force with incidence.
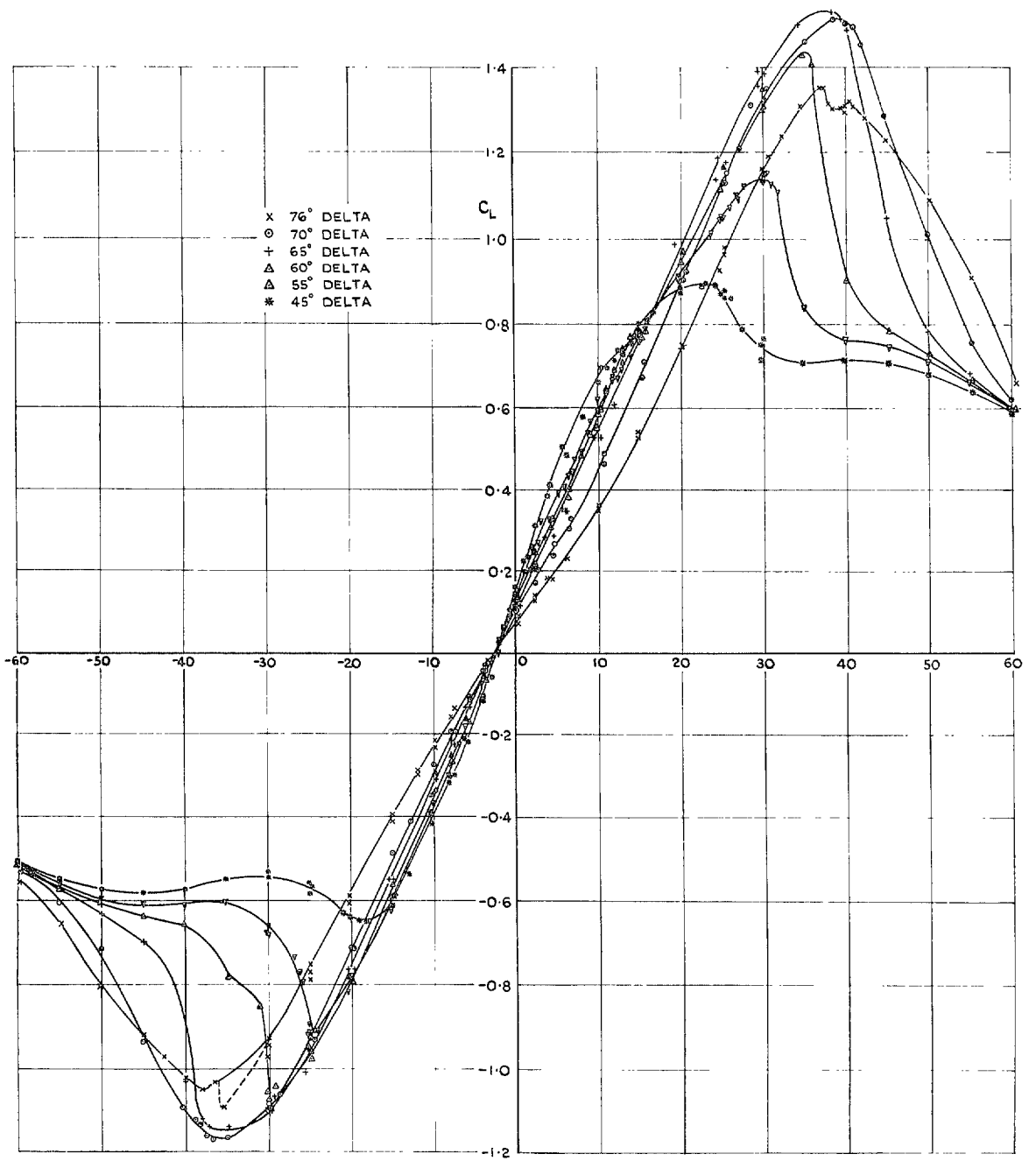
FIG. 4. Variation of lift with incidence.

16
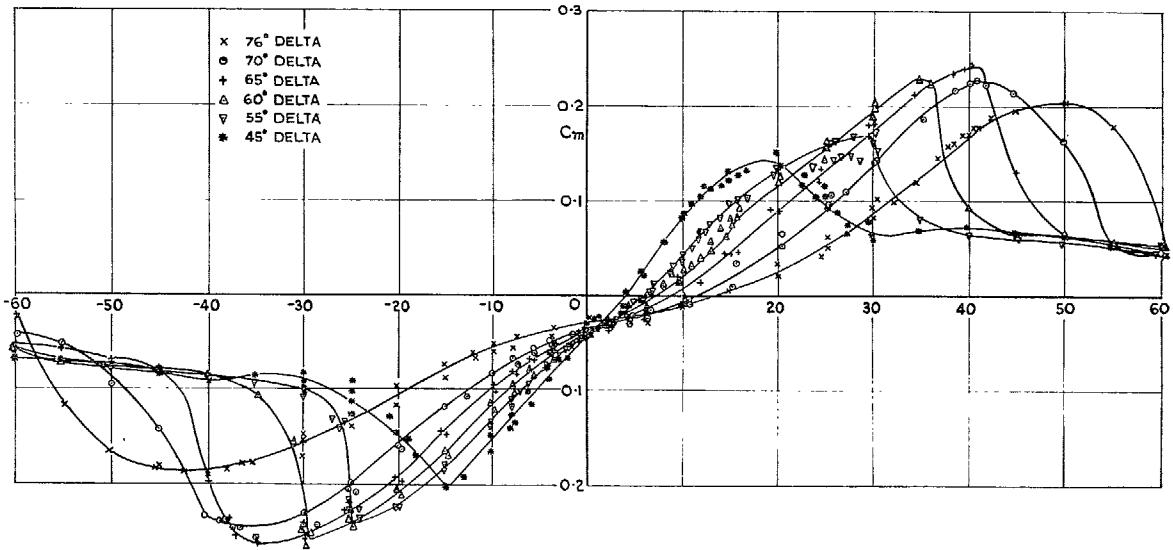
Fig. 5. Variation of pitching moment with incidence.
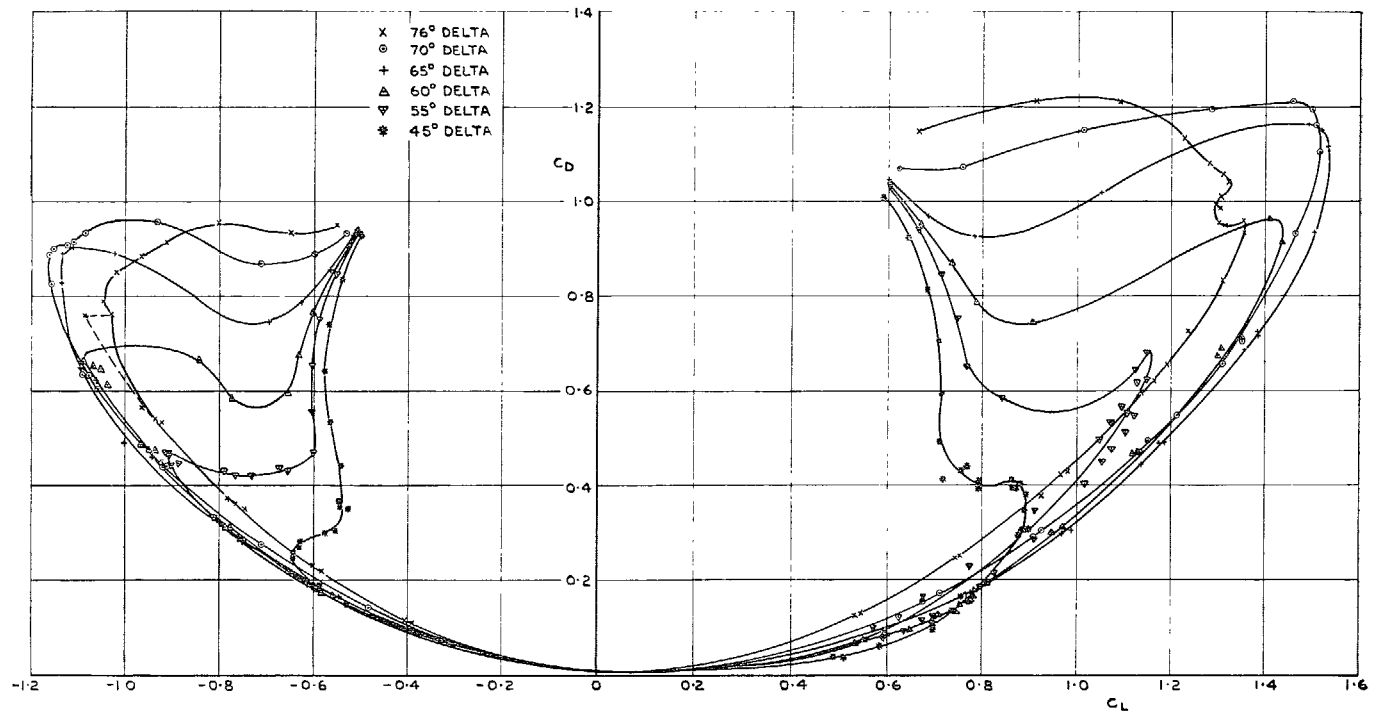
FIG. 6.   Variation of drag with lift.
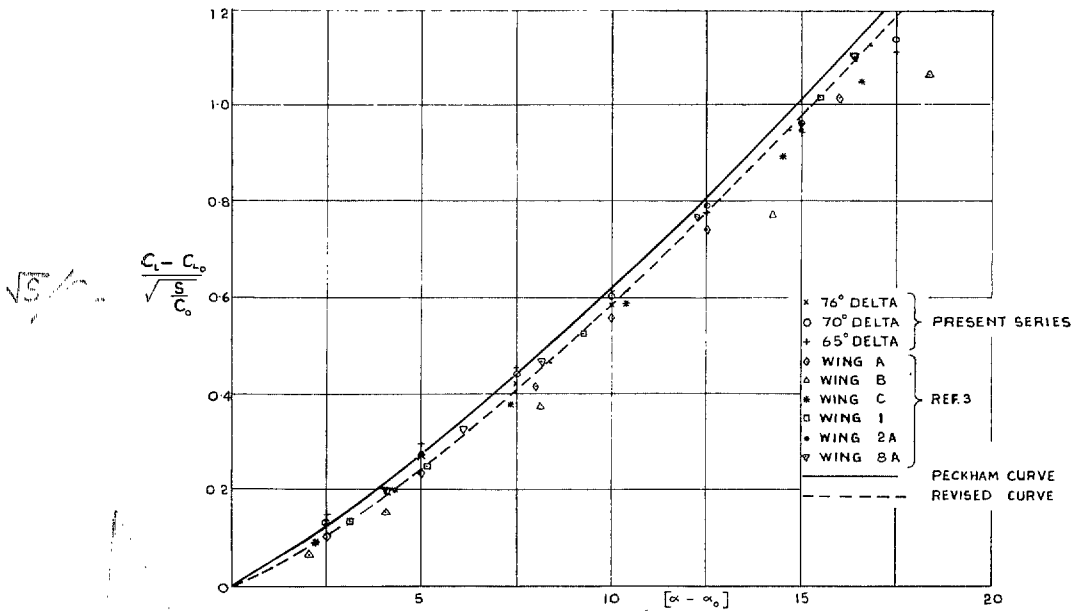
FIG. 7. Variation of $(C_L - C_{L0})/\sqrt{S/C_0}$ with $(\alpha - \alpha_0)$ for several gothic and delta wings.
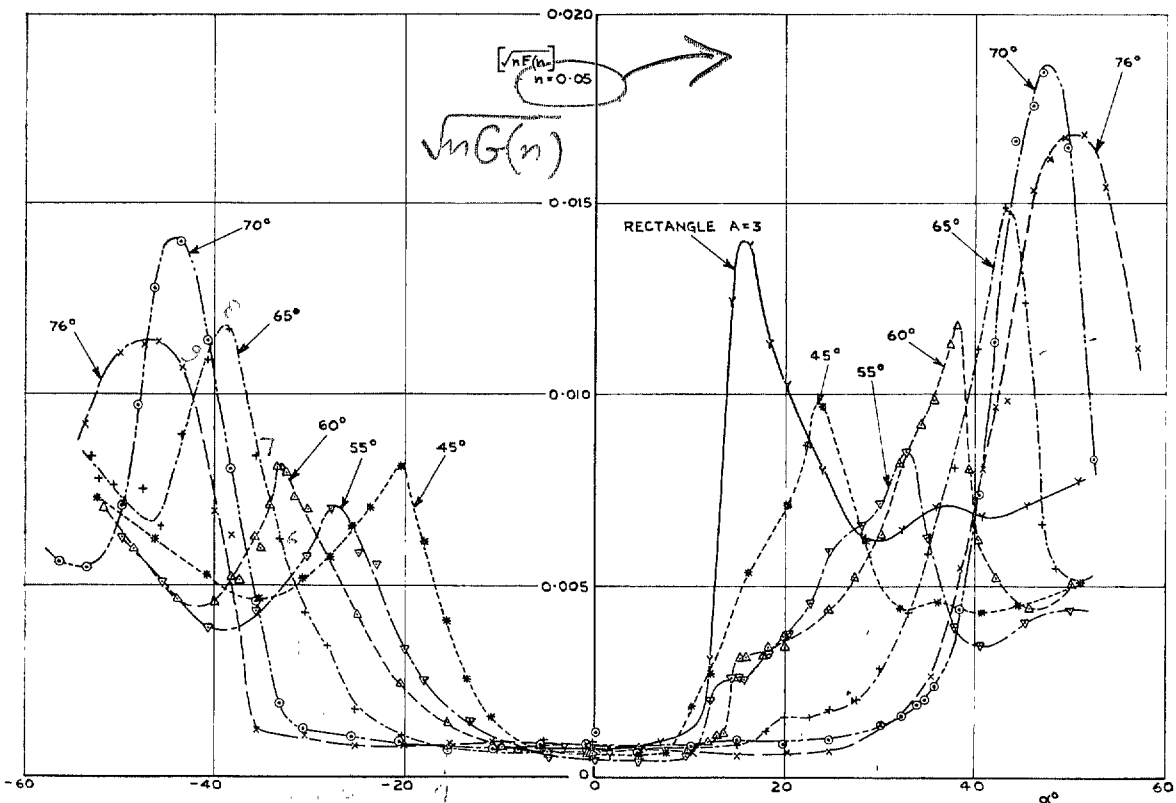
FIG. 8. Variation of low-frequency component of normal-force fluctuation with incidence.

19
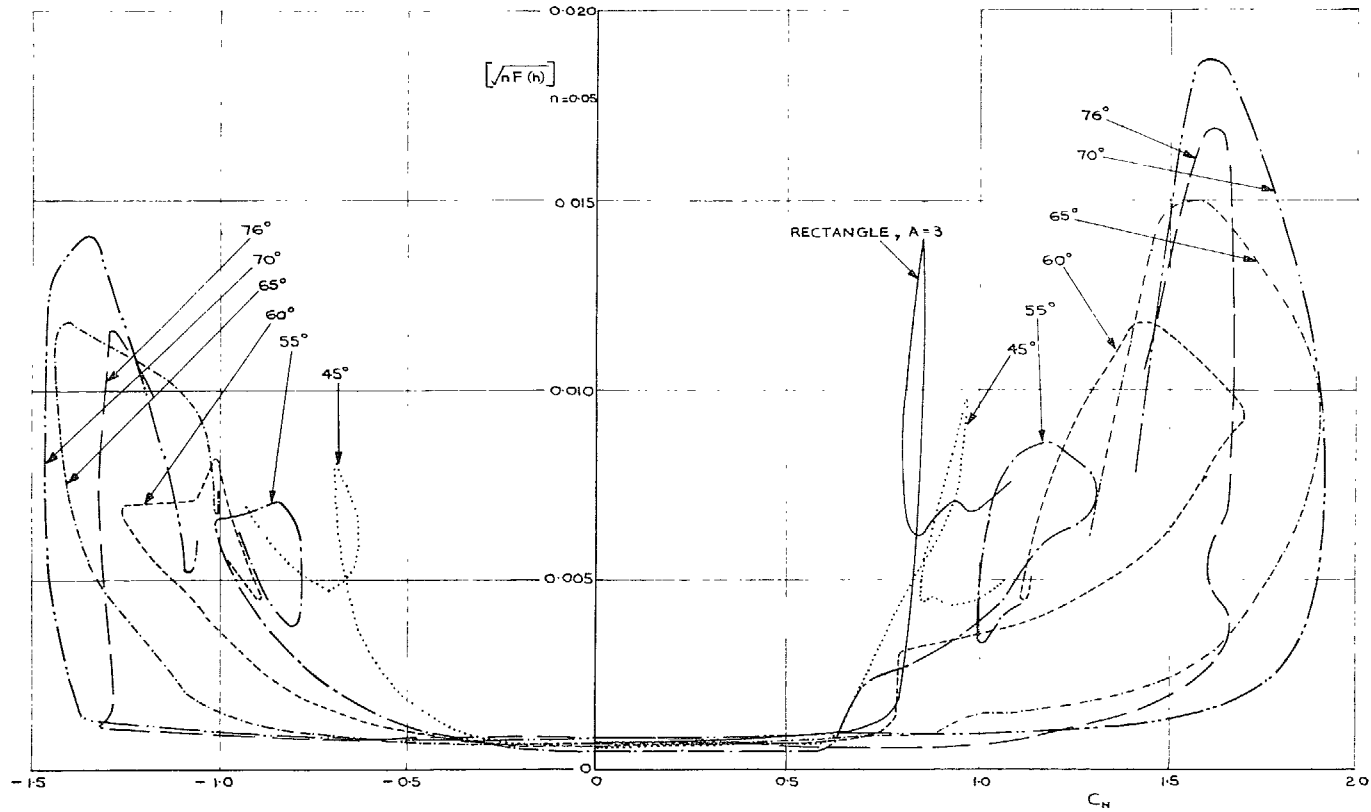
FIG. 9. Variation of low-frequency component of normal-force fluctuation with normal force.
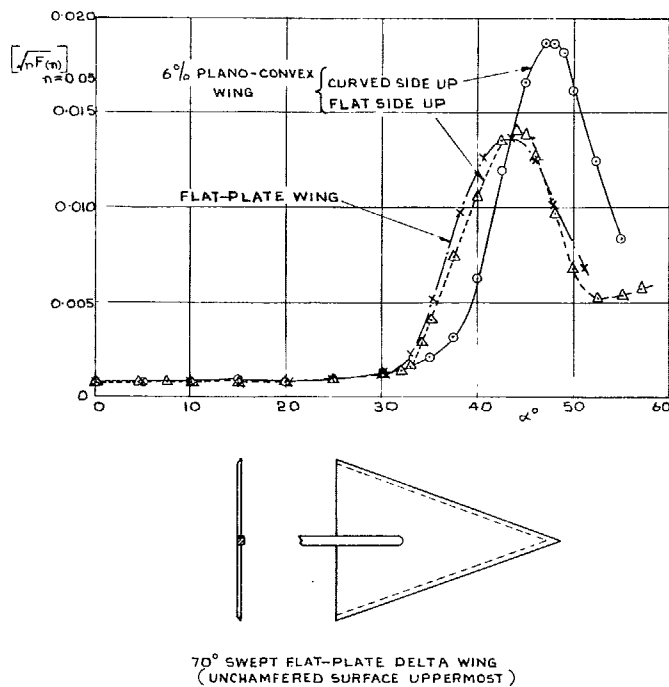
FIG. 10. Low-frequency component of normal-force fluctuations on delta wings with 70° leading-edge sweepback.
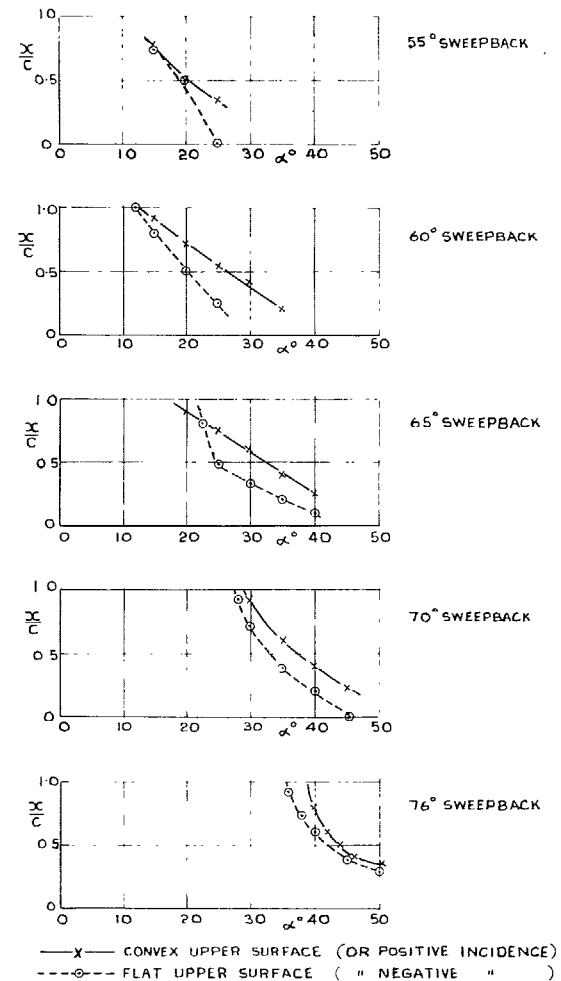
FIG. 11. Chordwise position of vortex breakdown point in terms of the centre-line chord.
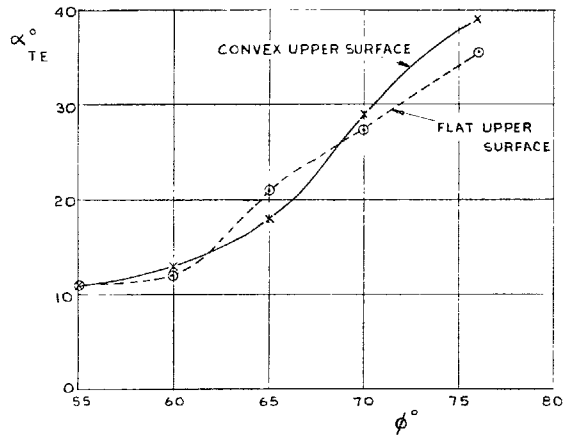
α_{TE} = INCIDENCE FOR VORTEX BREAKDOWN IN THE PLANE
OF THE TRAILING EDGE

ϕ = LEADING-EDGE SWEEPBACK ANGLE

FIG. 12. Relation between incidence for
vortex breakdown in plane of trailing edge,
and angle of leading-edge sweepback.
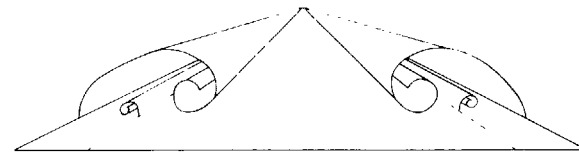
(a) VORTEX SHEETS FORMED ABOVE THE WING
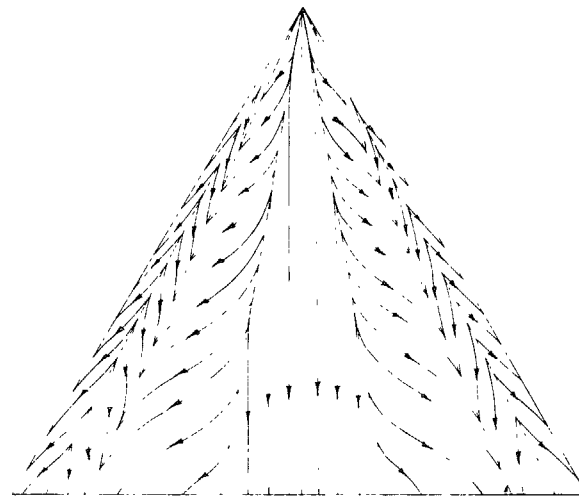
(b) SURFACE FLOW PATTERN

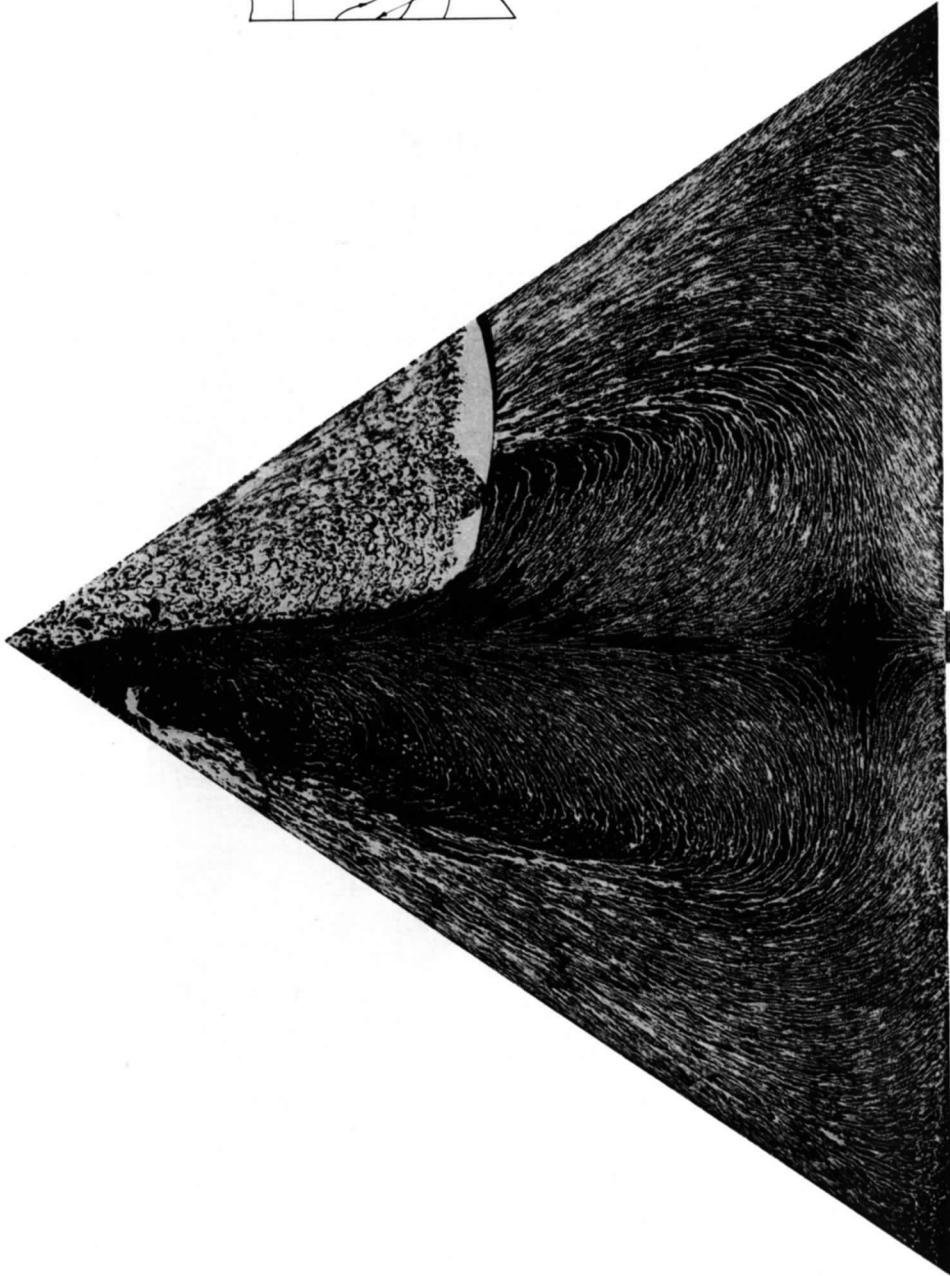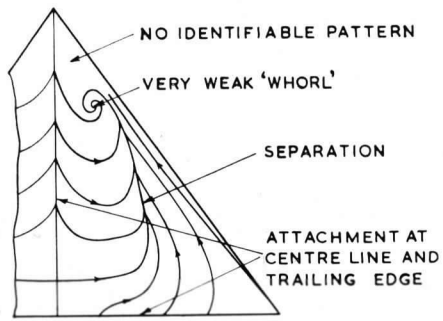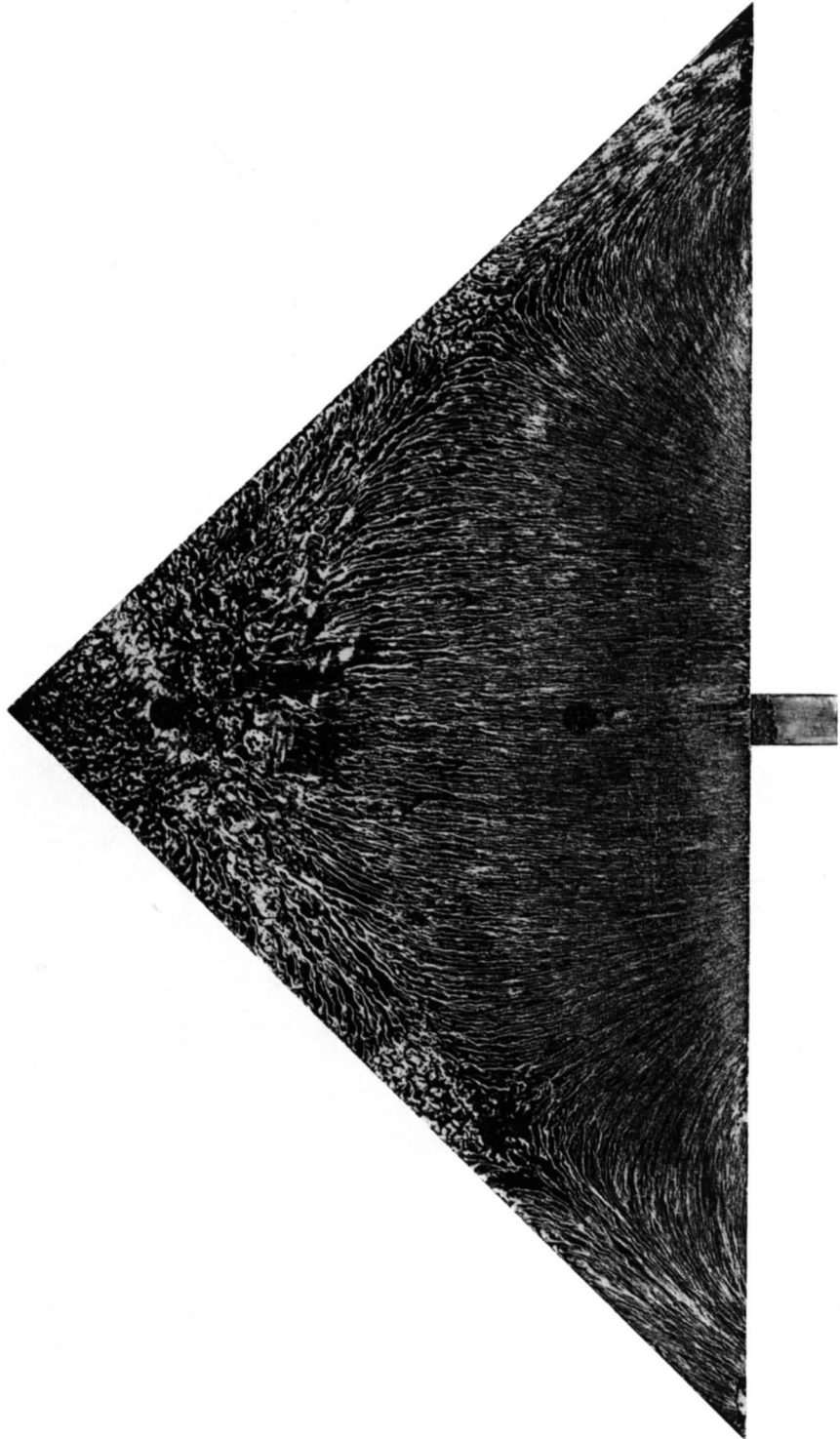FIG. 13. Typical flow over a delta wing at
moderate incidence.
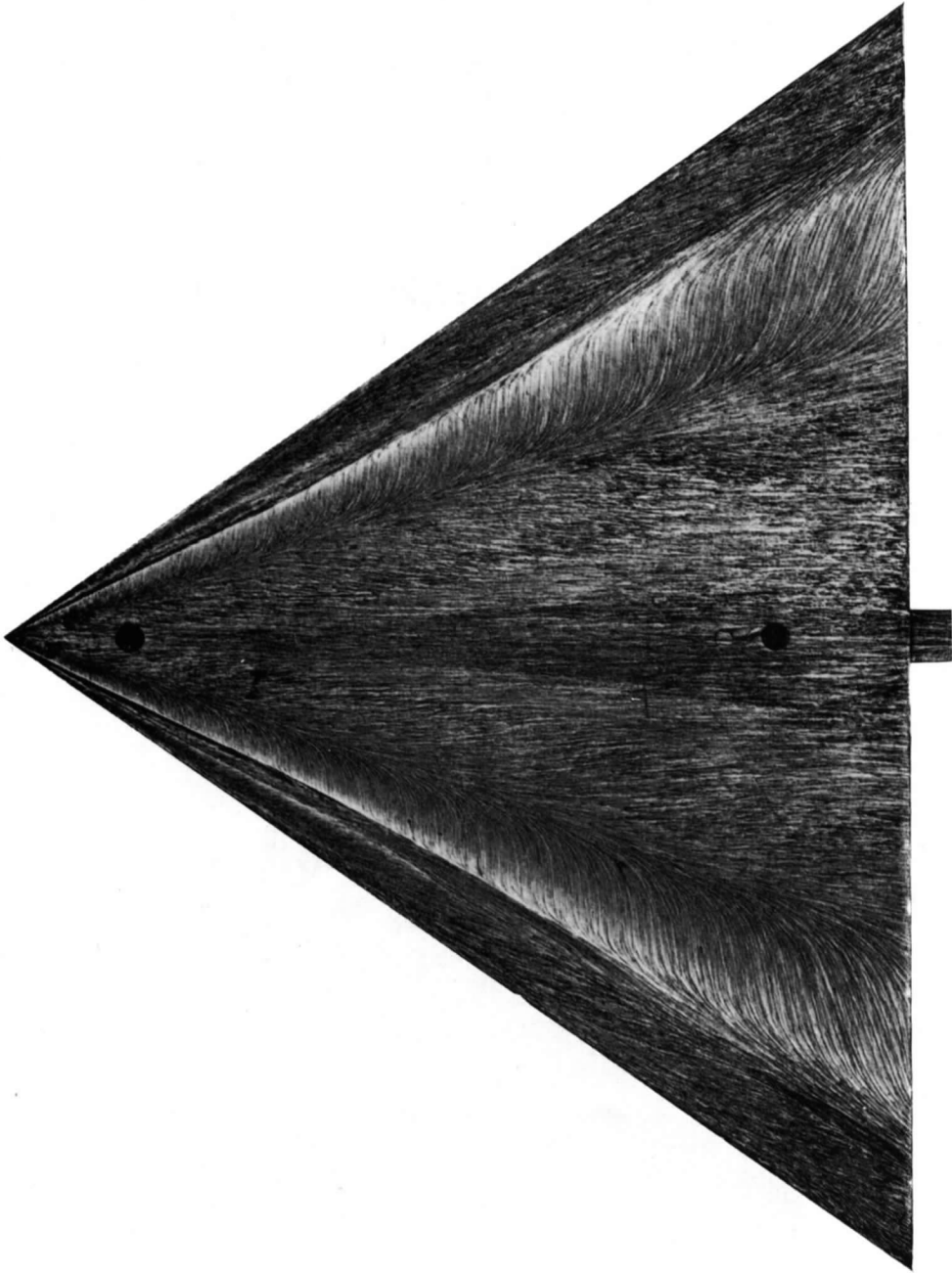
FIG. 14. 55° delta wing, flat upper surface. Oil-flow pattern at $\alpha = 10°$.

23
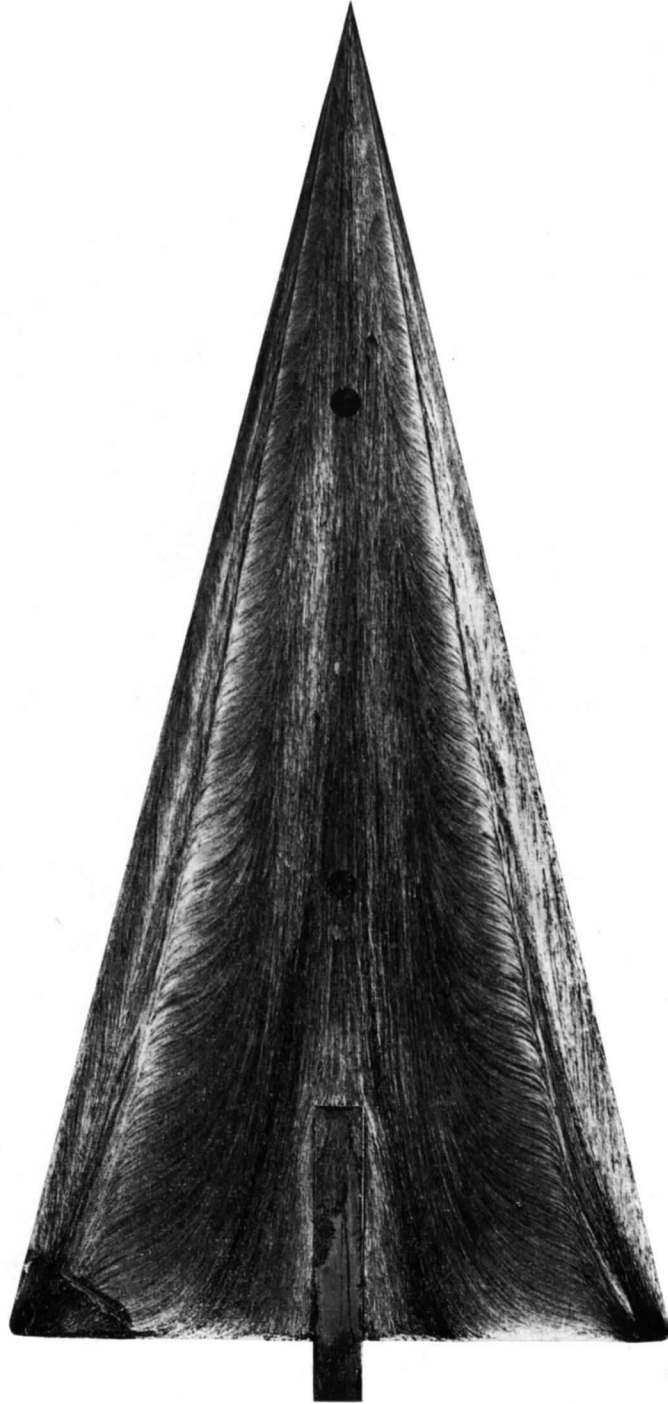
Fig. 15.   76° delta wing, convex upper surface. Oil-flow
pattern at $\alpha = 20°$.
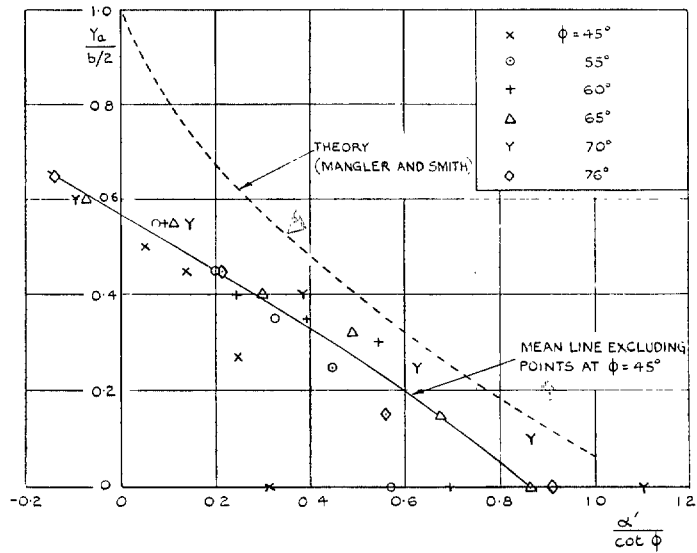
Y_a = DISTANCE FROM CENTRE LINE TO ATTACHMENT
b = LOCAL SPAN
α' = INCIDENCE (TAKEN FROM ZERO LIFT ANGLE, IN RADIANS)
ϕ = LEADING-EDGE SWEEPBACK ANGLE

FIG. 16. Spanwise position of leading-edge vortex attachment line.
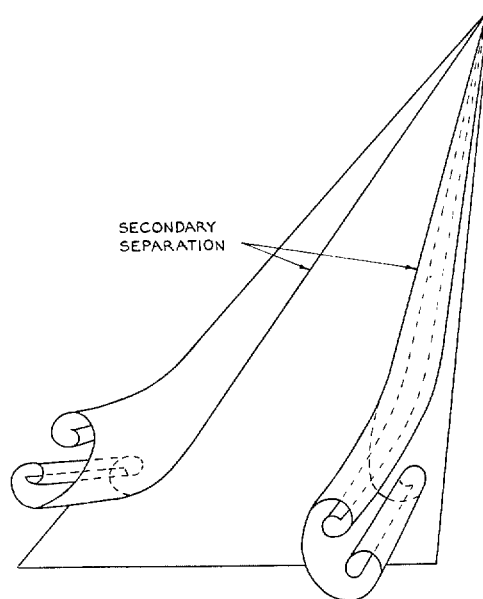
FIG. 17. Suggested secondary vortex system associated with 'whorl' surface pattern.

25
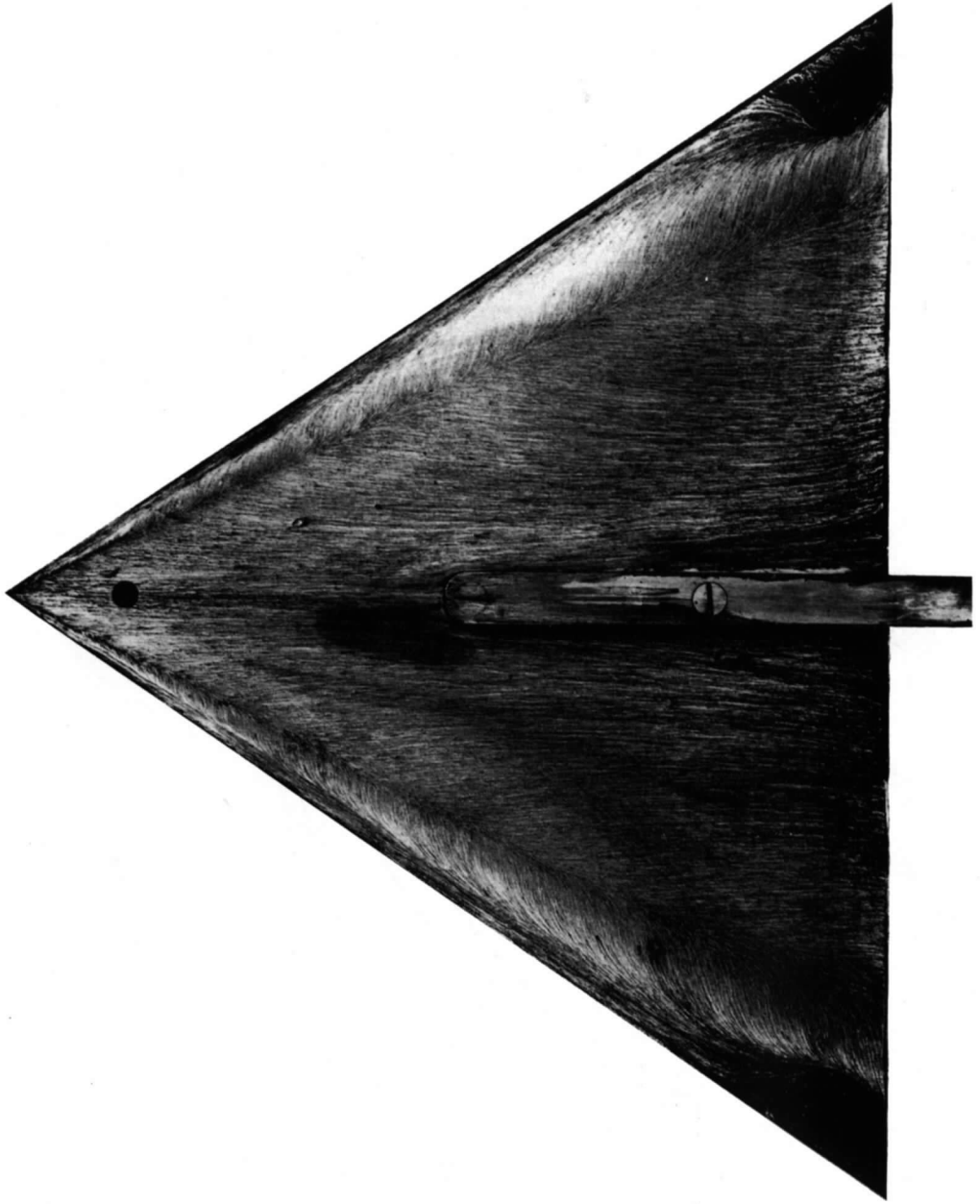
FIG. 18.   55° delta wing, convex upper surface.   Oil-flow pattern at $\alpha = 10°$.
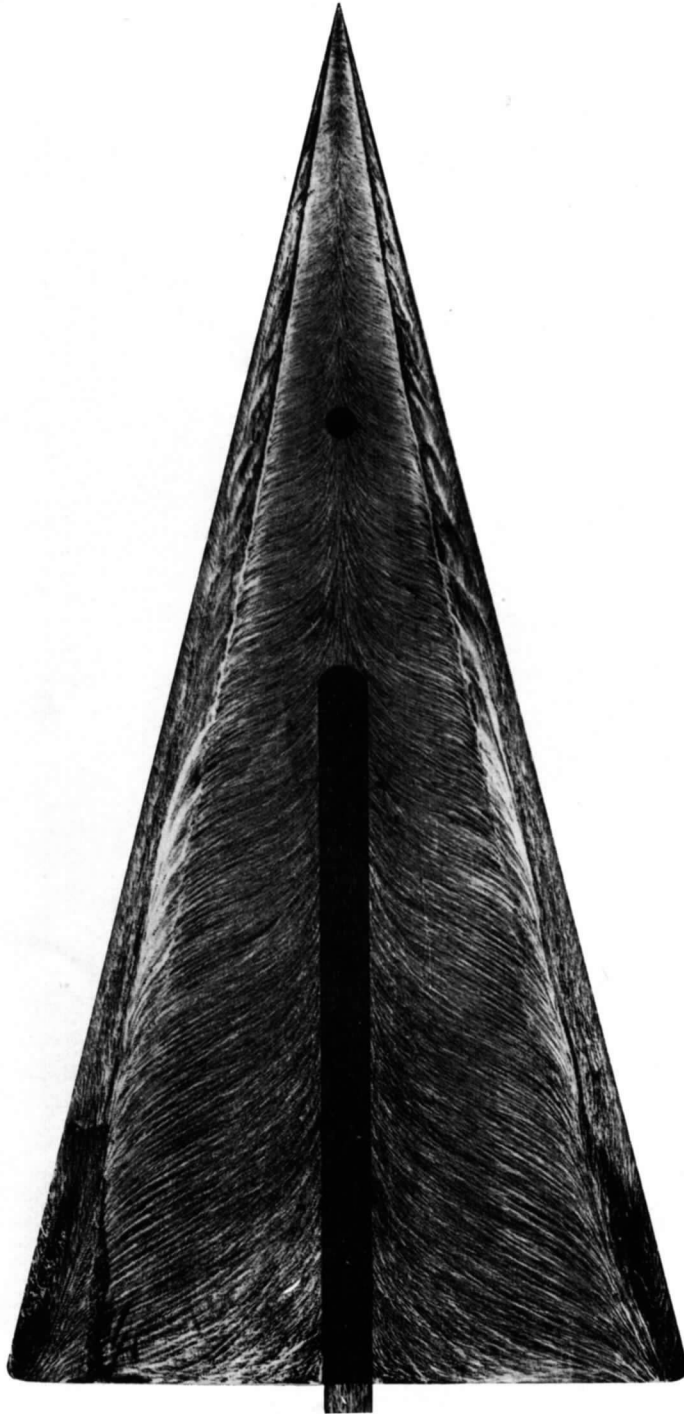
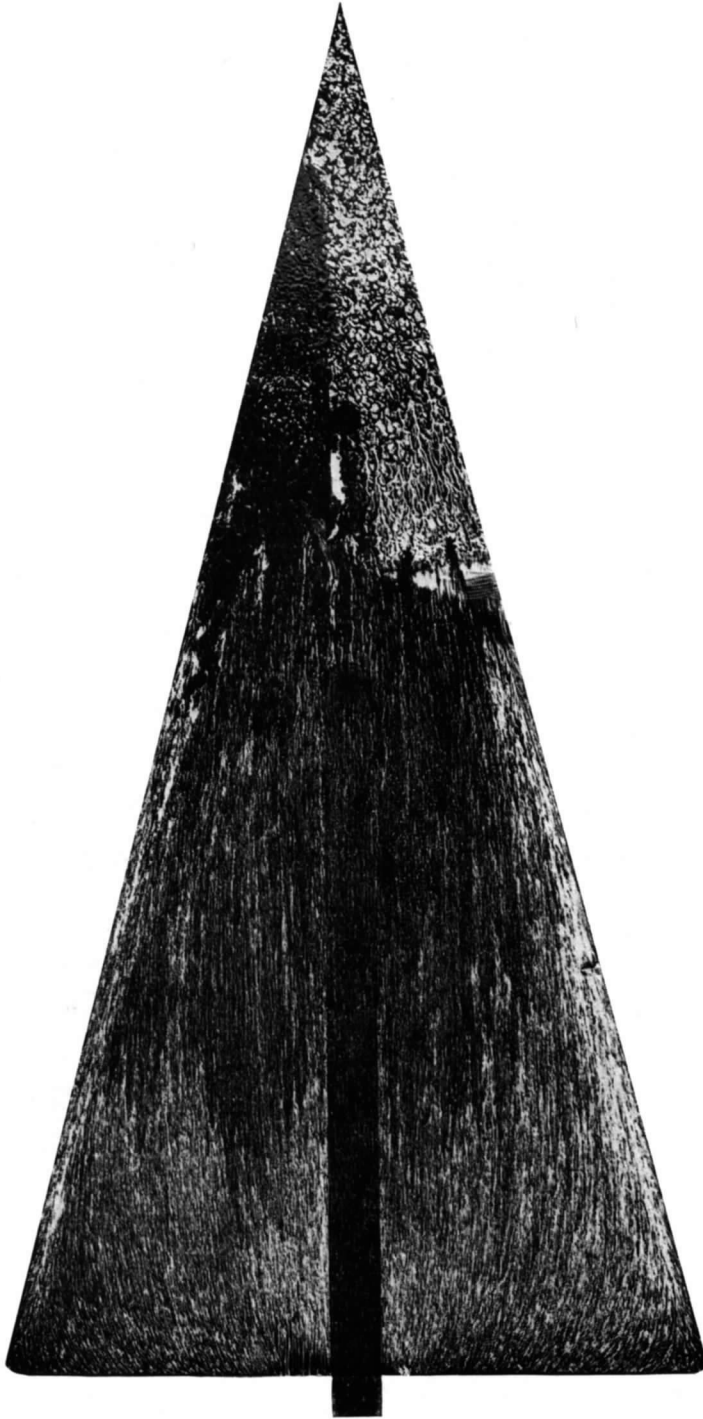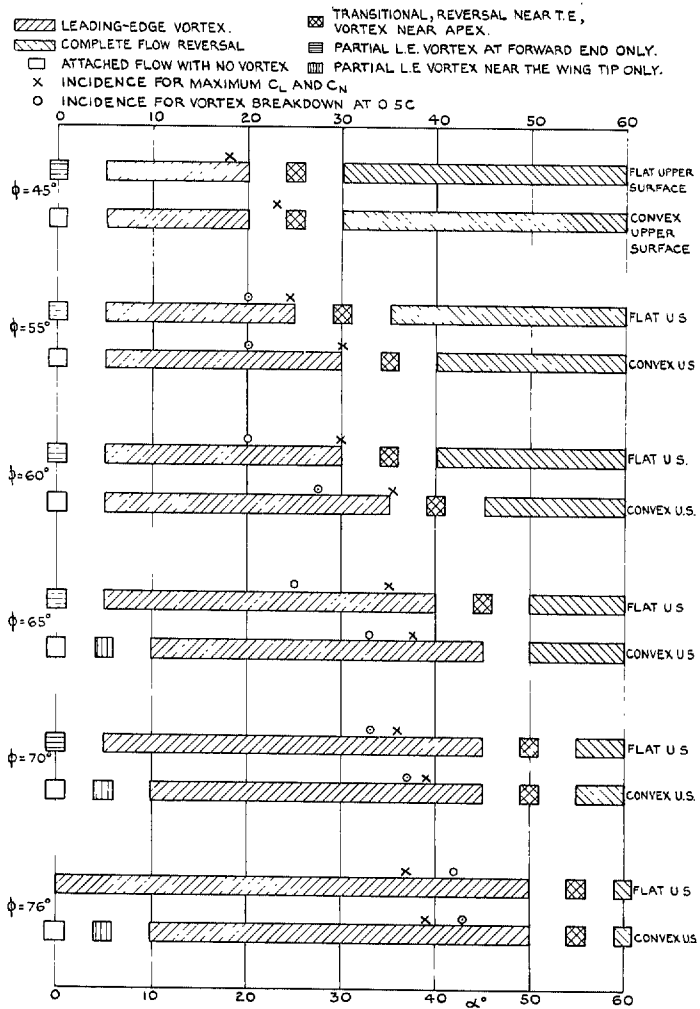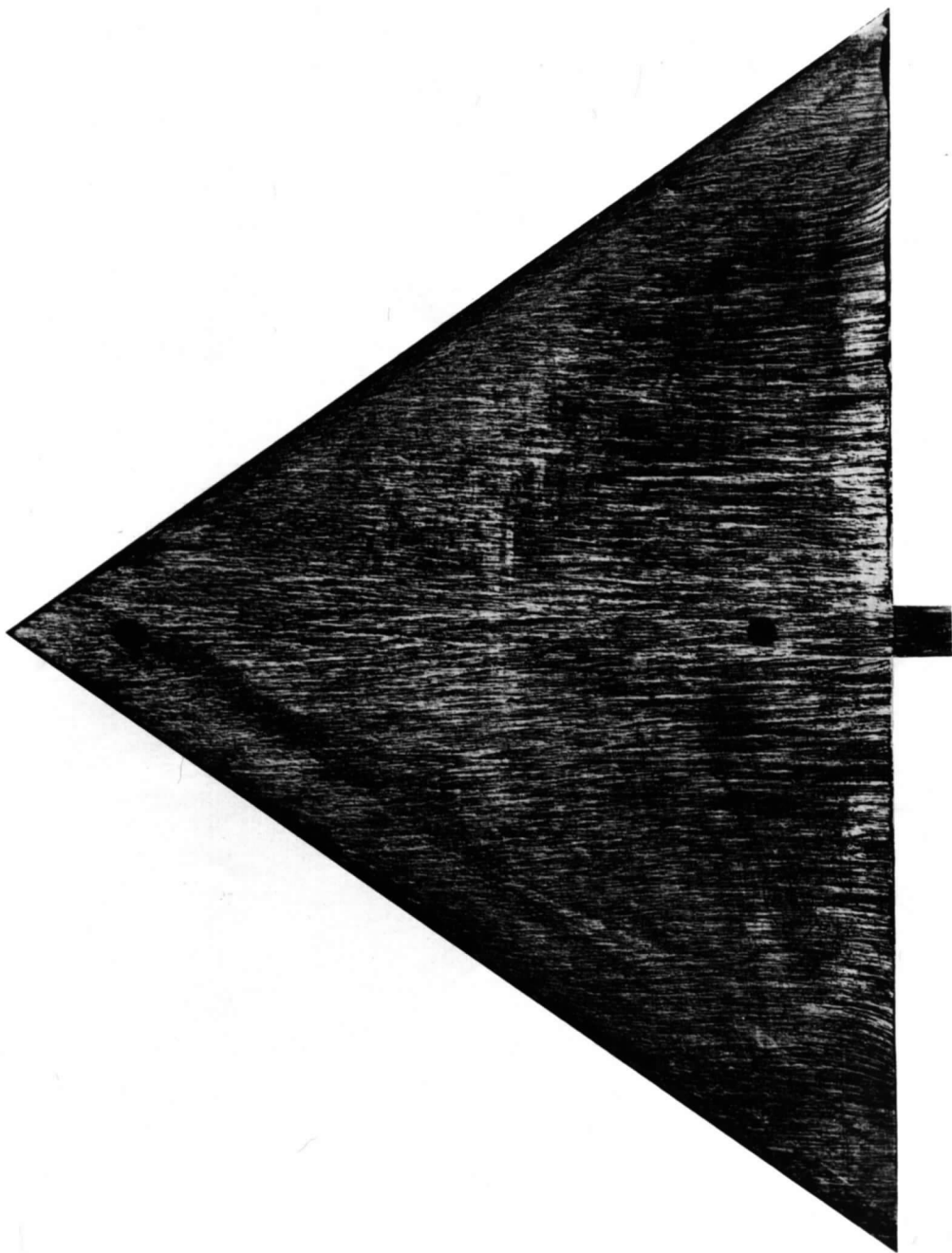Fig. 19.   76° delta wing, flat upper surface. Oil-flow pattern
at $\alpha = 35°$.
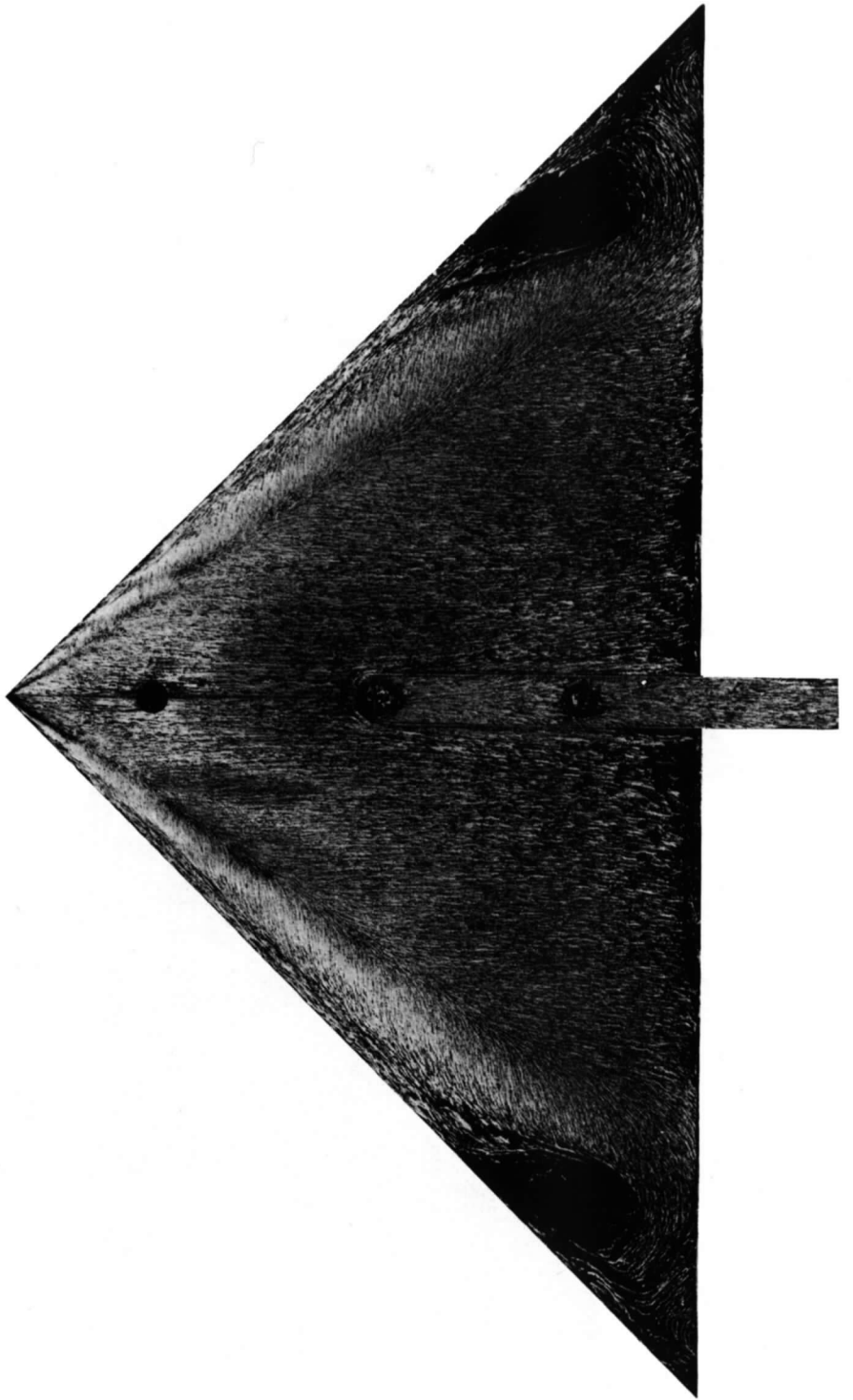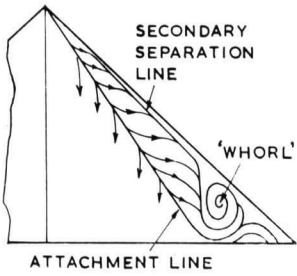
FIG. 20. 45° delta wing, convex upper surface. Oil-flow pattern at $\alpha = 10°$.

CENTRE–LINE
ATTACHMENT

SECONDARY
SEPARATION LINE

TRAILING–EDGE ATTACHMENT
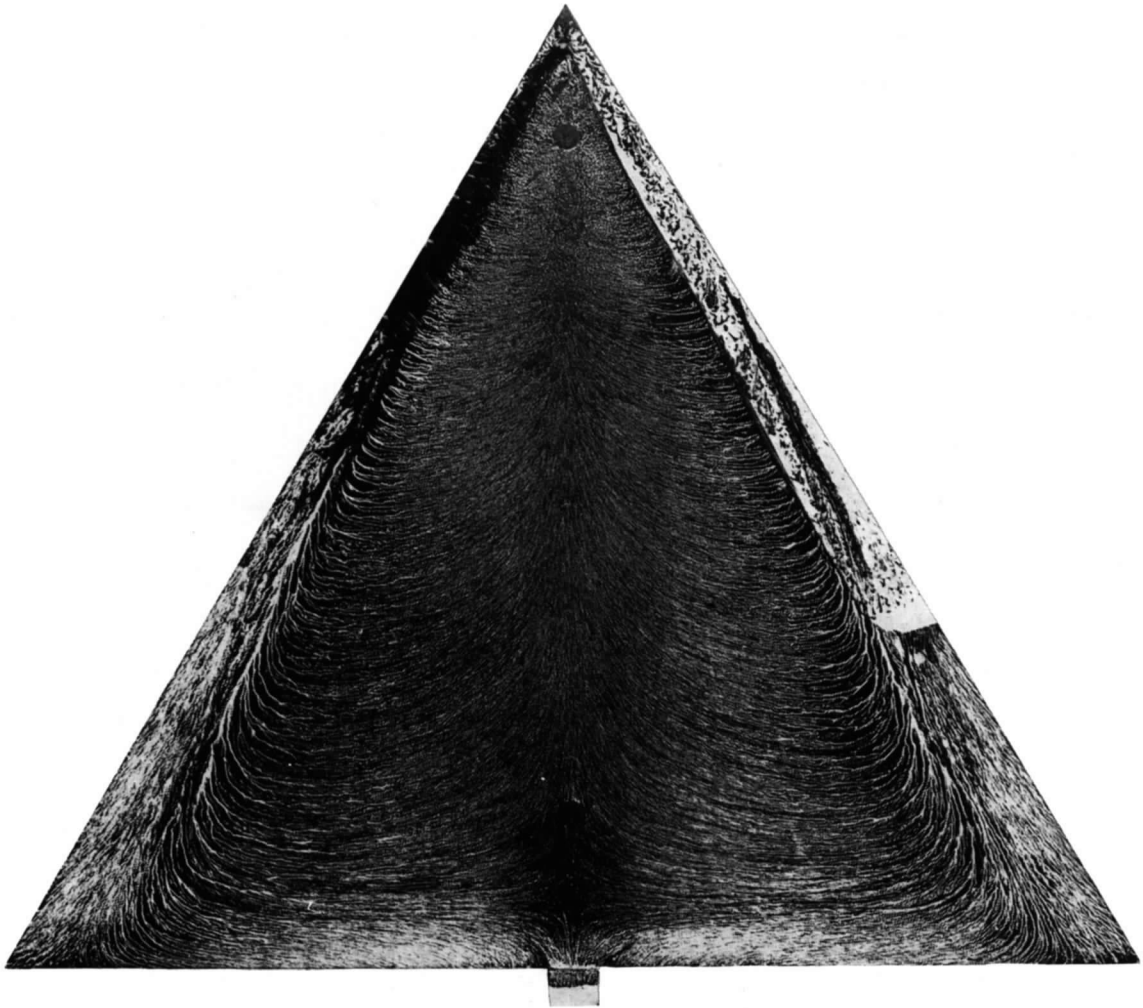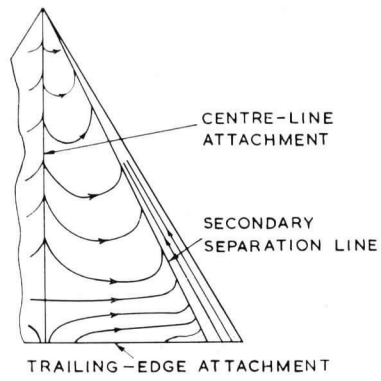
FIG. 21.   60° delta wing, flat upper surface. Oil-flow pattern at $\alpha = 35°$.
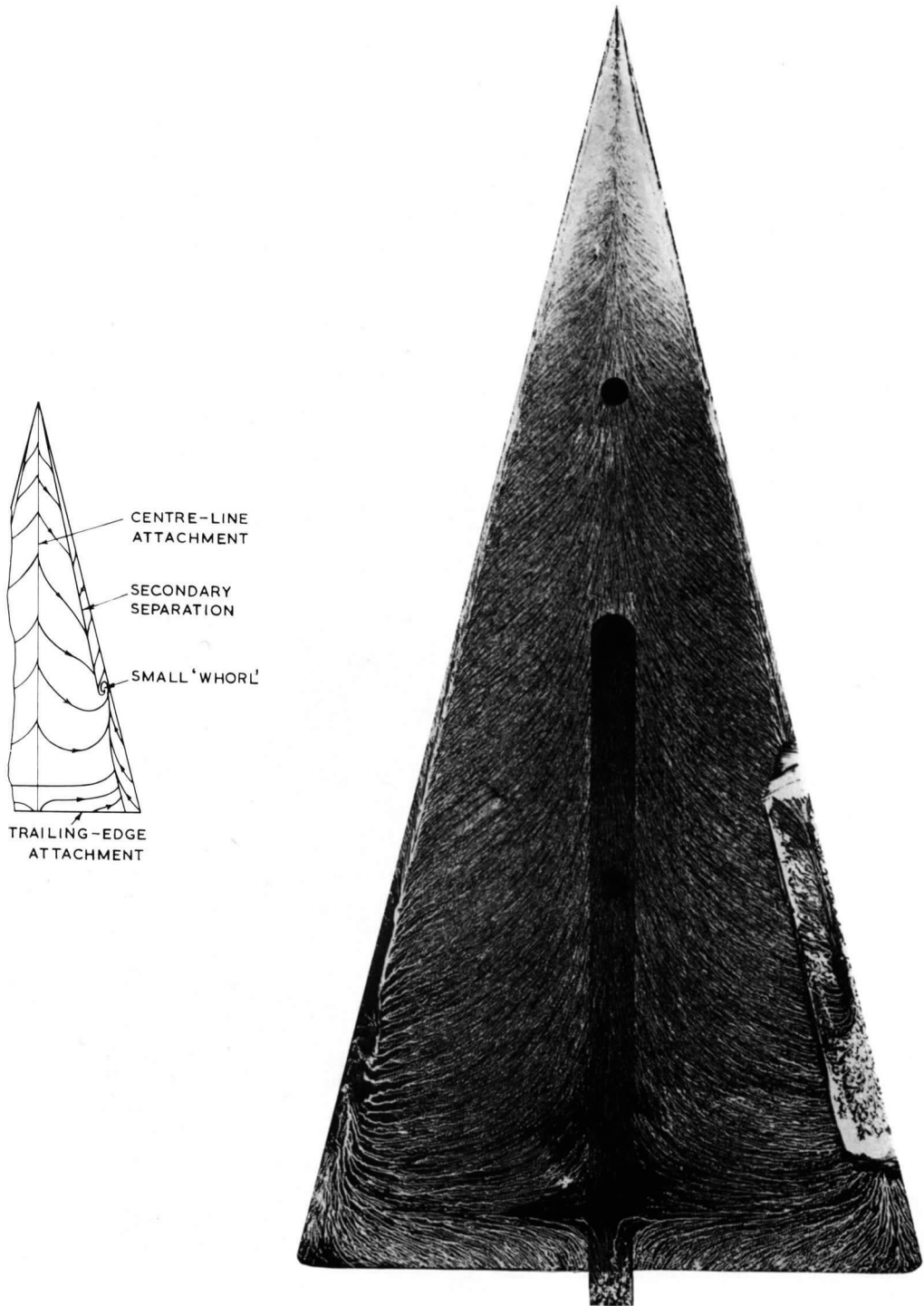
FIG. 22.   76° delta wing, flat upper surface. Oil-flow pattern at $\alpha = 55°$.

Labels on diagram:
CENTRE-LINE ATTACHMENT
SECONDARY SEPARATION
SMALL 'WHORL'
TRAILING-EDGE ATTACHMENT

NO IDENTIFIABLE PATTERN

VERY WEAK 'WHORL'

SEPARATION

ATTACHMENT AT
CENTRE LINE AND
TRAILING EDGE

FIG. 23.   55° delta wing, flat upper surface. Oil-flow pattern at $\alpha = 30°$.

31

FIG. 24. 45° delta wing, flat upper surface. Oil-flow pattern at $\alpha = 35°$.

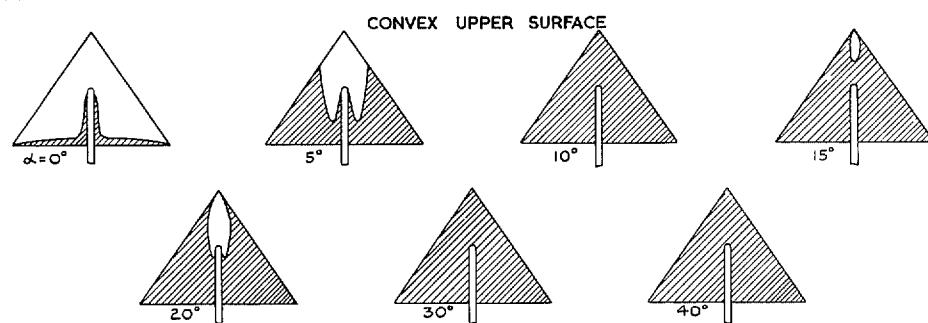FIG. 25. 76° delta wing, flat upper surface. Oil-flow pattern at
$\alpha = 60°$.

33

FIG 26. Variation of surface flow pattern type with incidence.

34

FIG. 27. 55° delta wing, flat lower surface. Oil-flow pattern at $\alpha = 10°$.
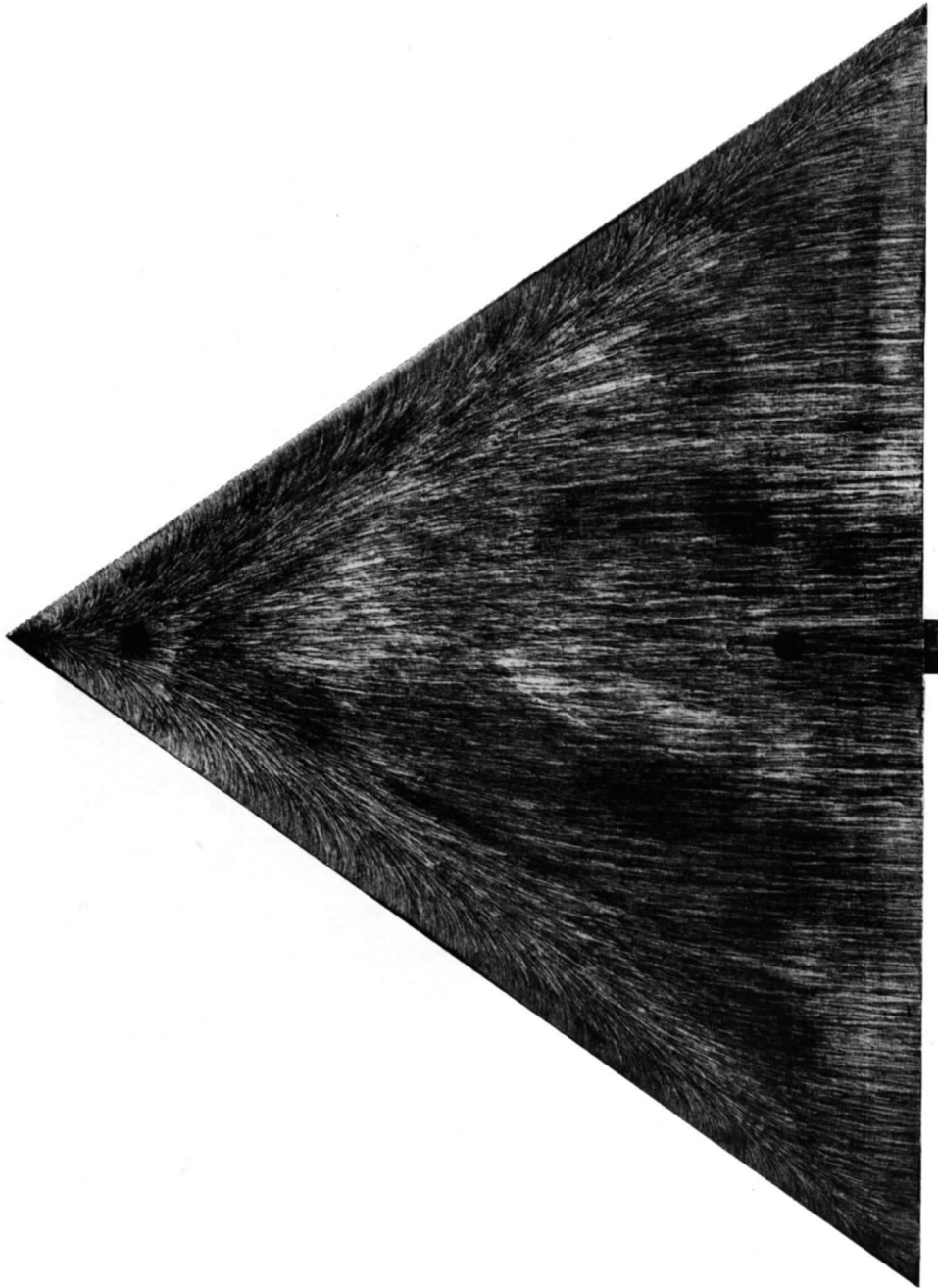
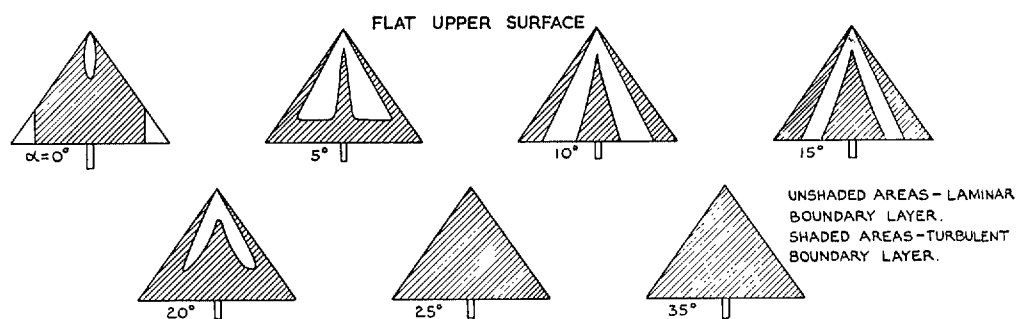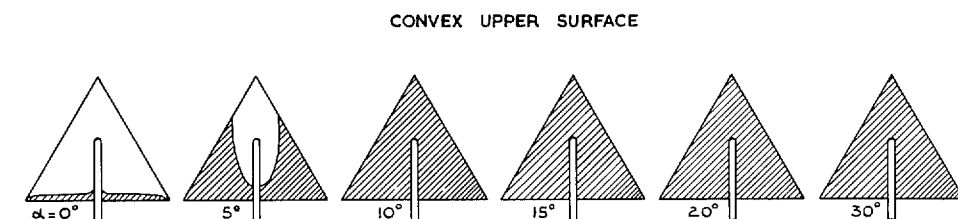FIG. 28. 55° delta wing, flat lower surface. Oil-flow pattern at $\alpha = 40°$.
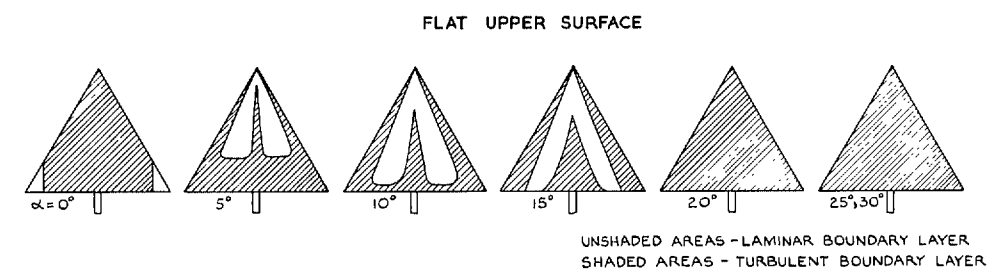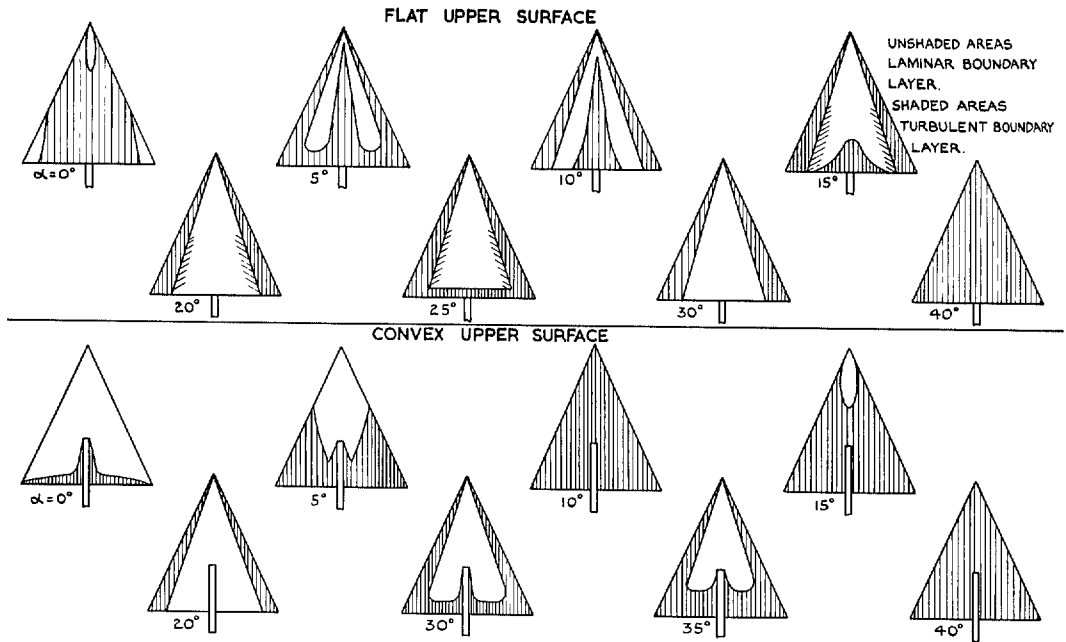
FIG. 29. Transition patterns on 55° delta wing.

FIG. 30. Transition patterns on 60° delta wing.

37

FIG. 31. Transition patterns on 65° delta wing.
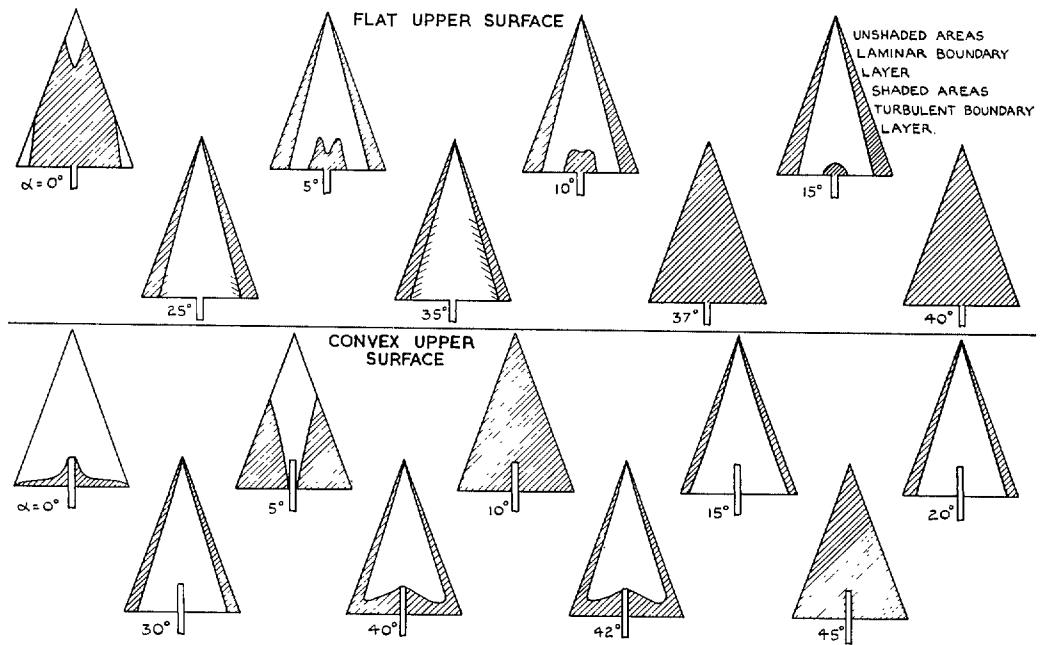
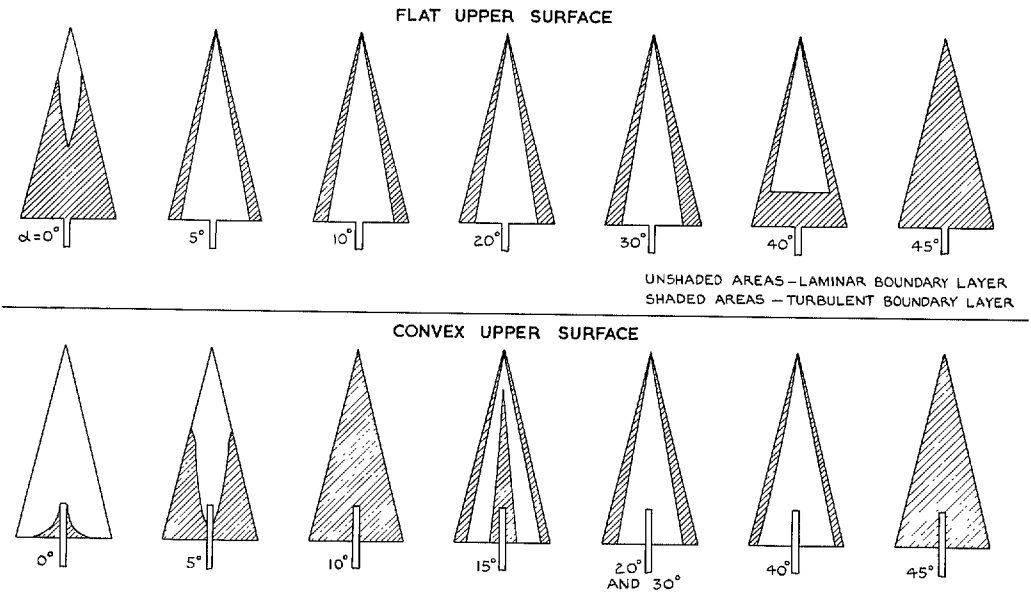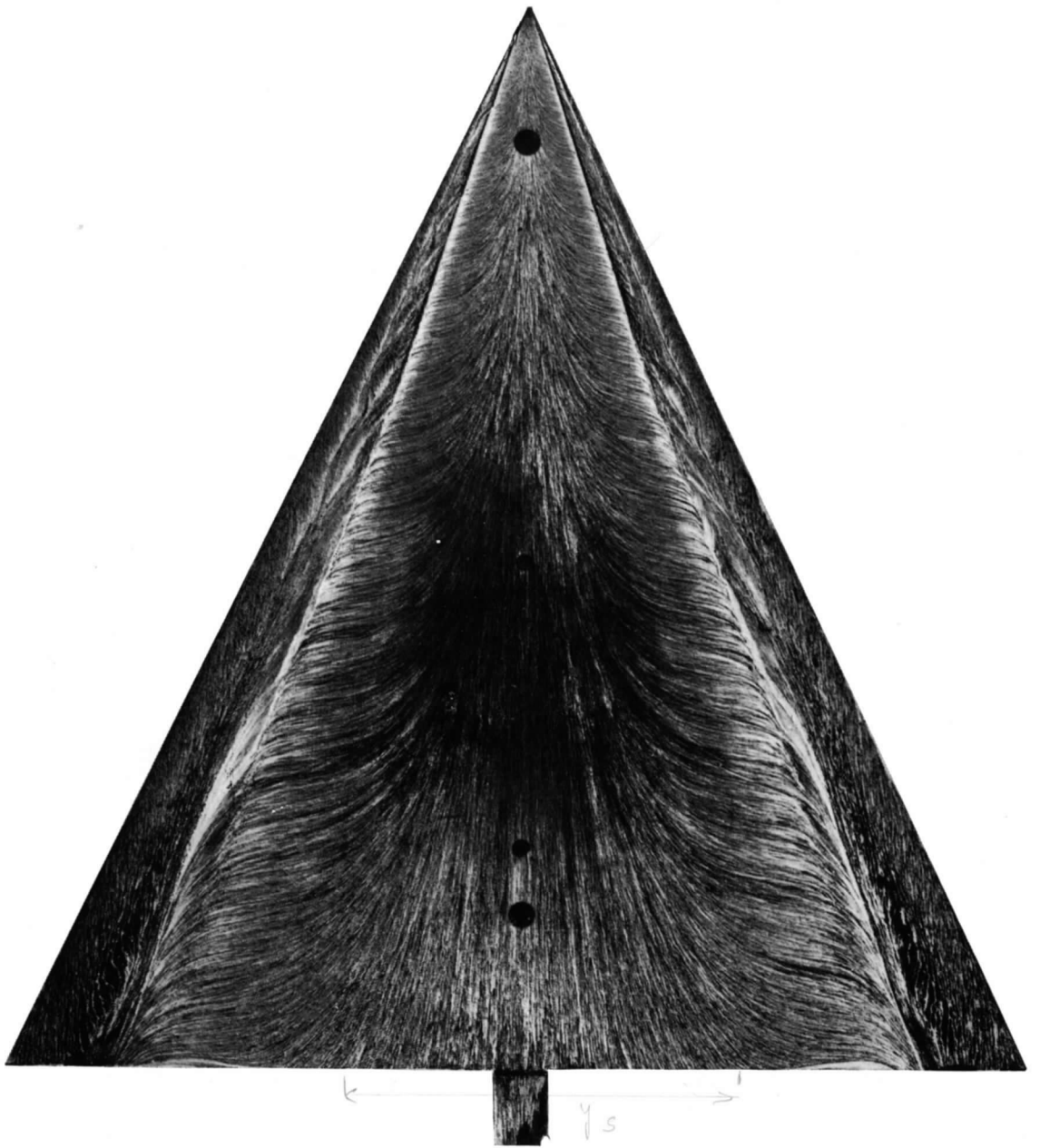FIG. 32. Transition patterns on 70° delta wing.

38

FLAT UPPER SURFACE

UNSHADED AREAS – LAMINAR BOUNDARY LAYER
SHADED AREAS – TURBULENT BOUNDARY LAYER

CONVEX UPPER SURFACE

FIG. 33.   Transition patterns on 76° delta wing.

39

Fig. 34a. 65° delta wing, flat upper surface. Oil-flow pattern at $\alpha = 20°$.

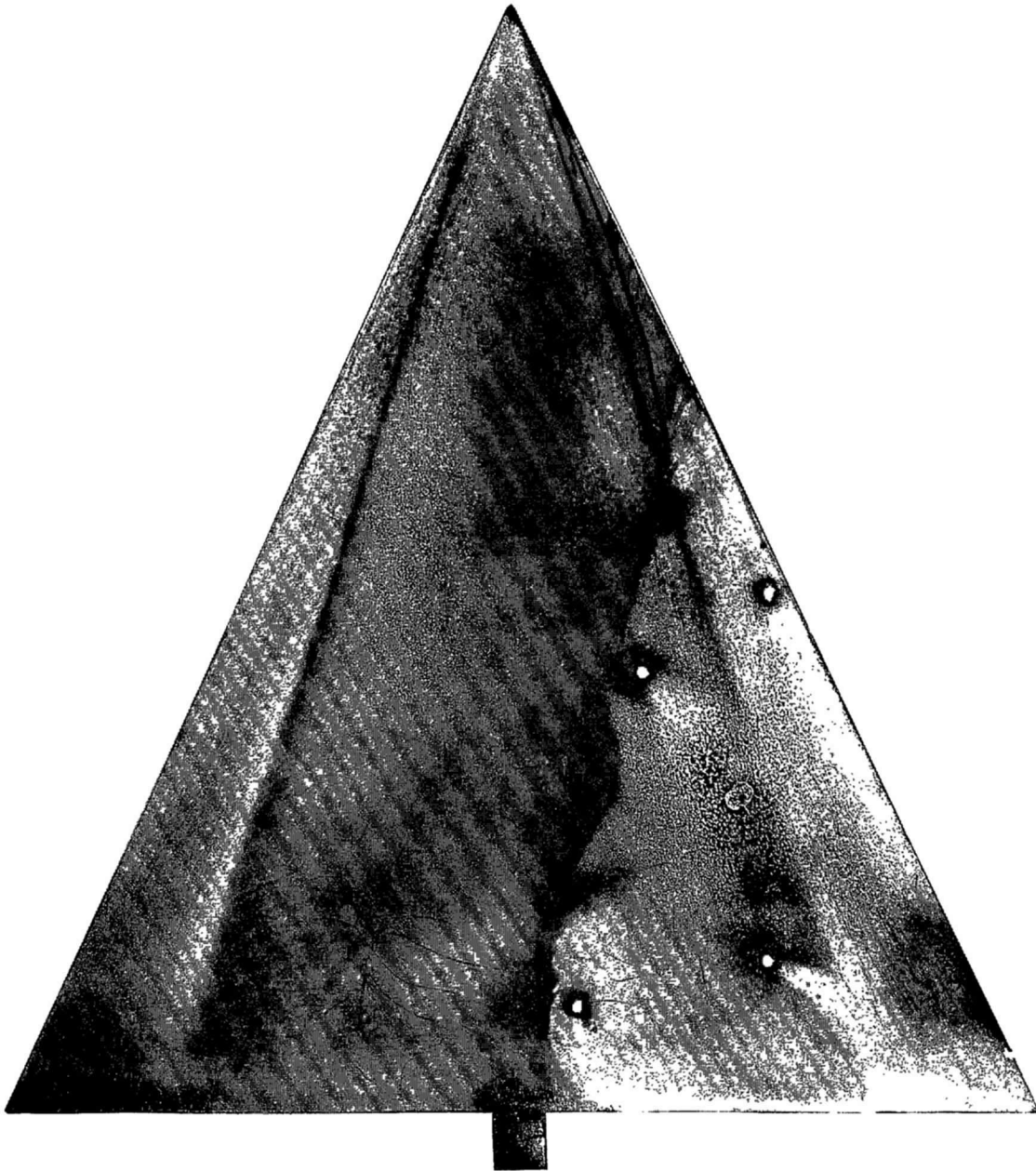$\alpha_0 = 17.5°$

40

$b = 146 mm$
$y_s = 56 mm$
$y/b = 0.38$

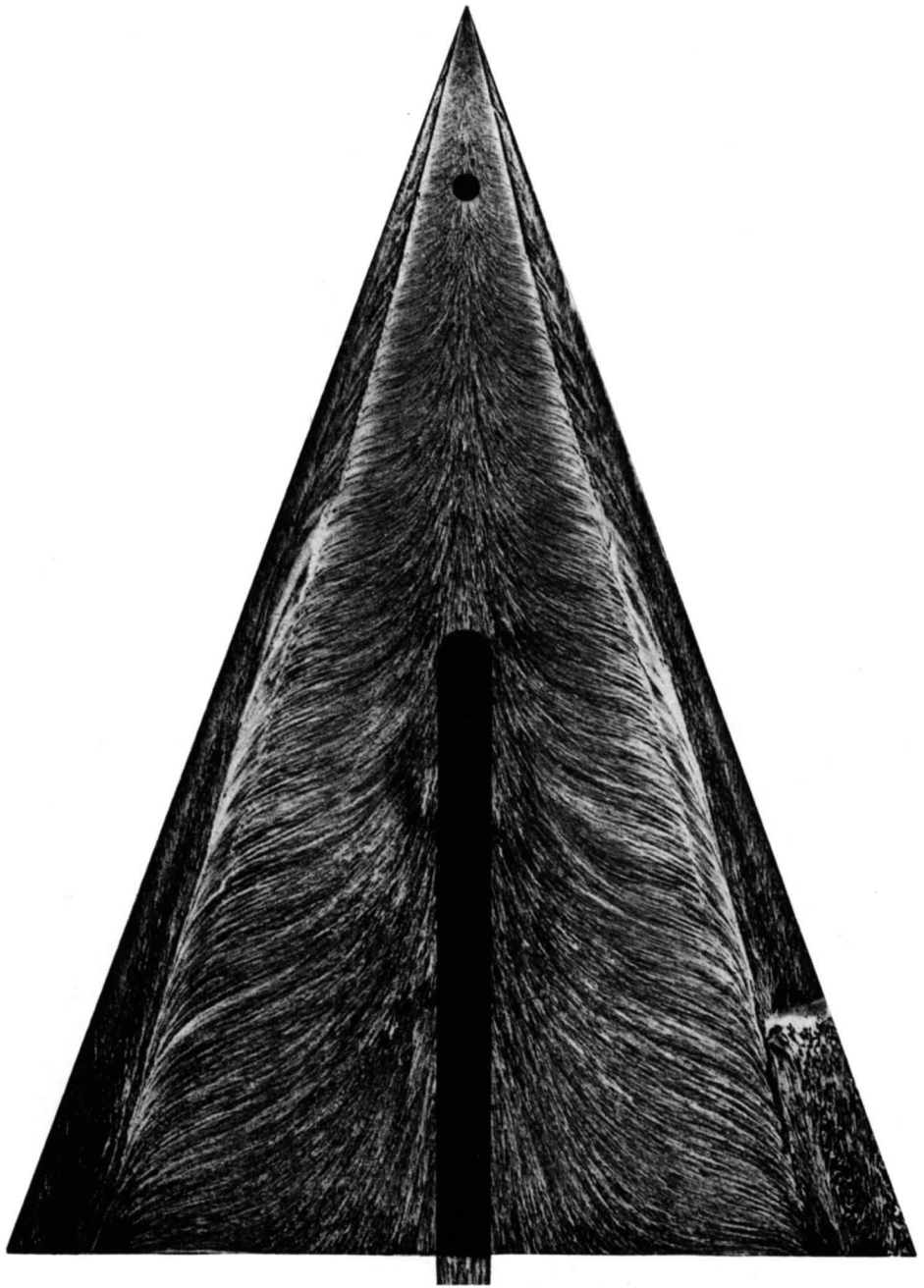FIG. 34b.   65° delta wing, flat upper surface. Transition pattern at $\alpha = 20°$.

41

FIG. 35a. 70° delta wing, flat upper surface. Oil-flow pattern at $\alpha = 25°$.

FIG. 35b.   70° delta wing, flat upper surface. Transition pattern at $\alpha = 25°$.
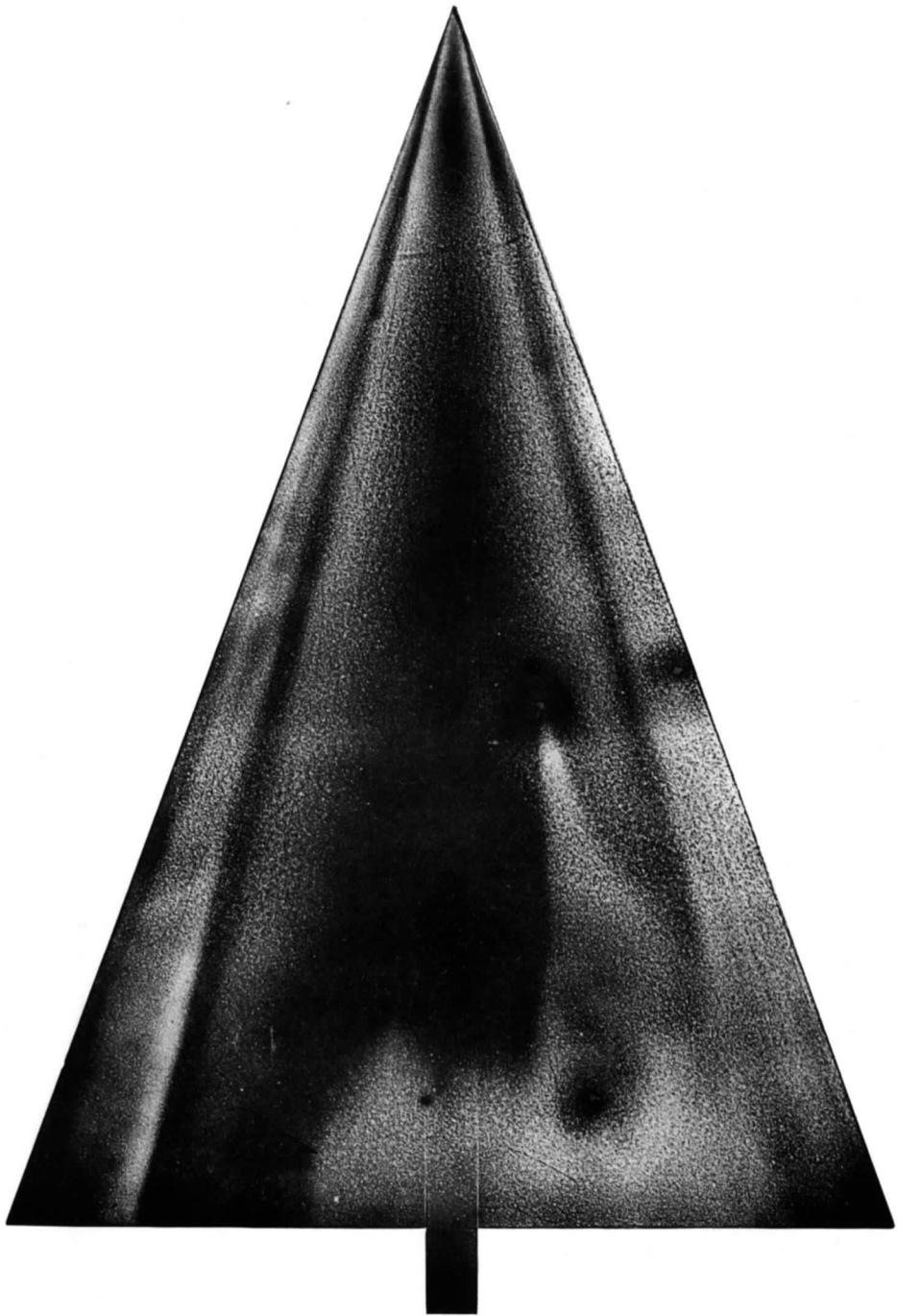
FIG. 36. 70° delta wing, flat upper surface. Transition pattern at $\alpha = 10°$.
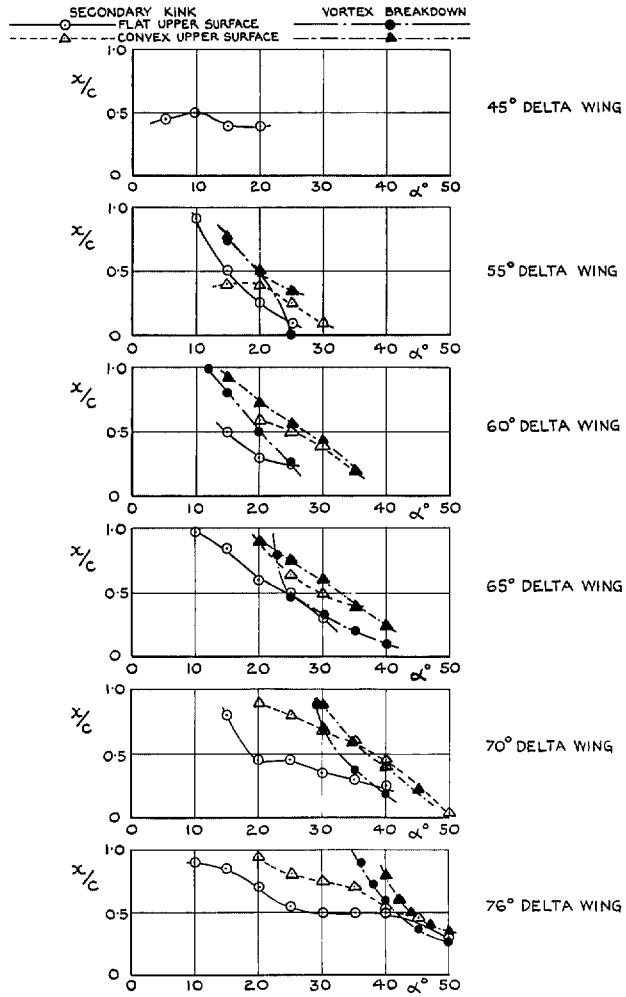
44

FIG. 37. Chordwise positions
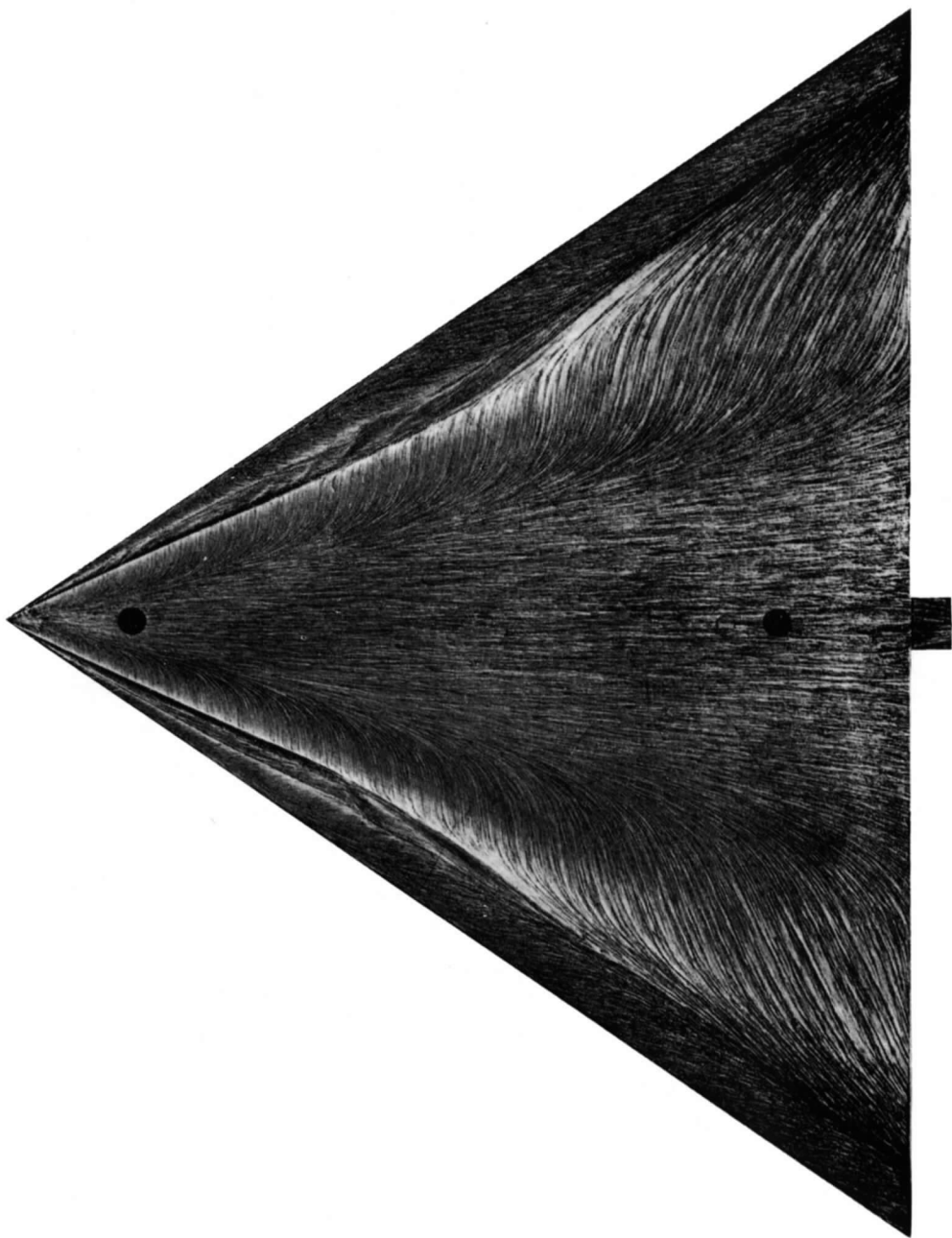of vortex breakdown point and
of secondary separation kink.

FIG. 38. 55° delta wing, flat upper surface. Oil-flow pattern at $\alpha = 15°$.

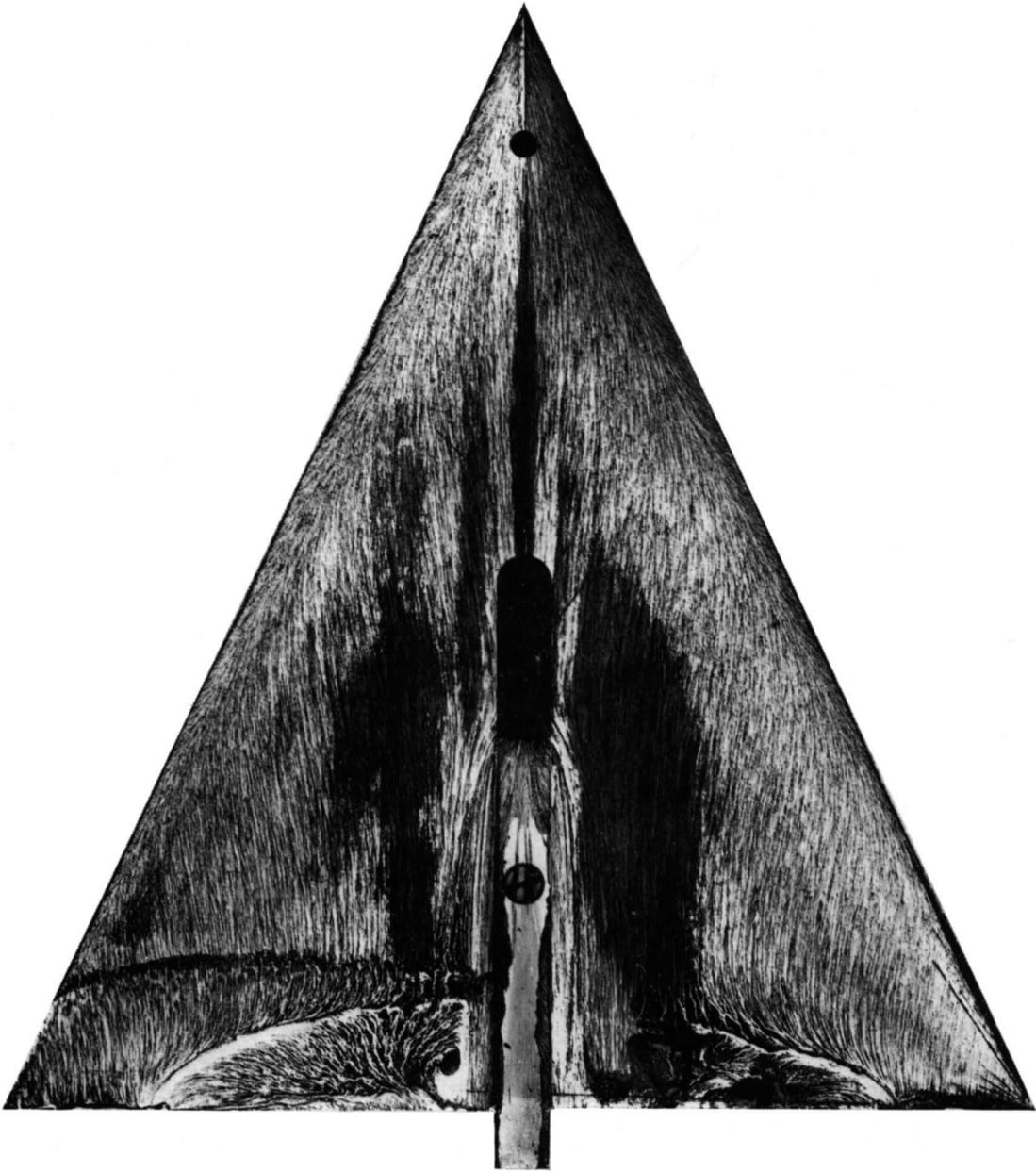FIG. 39. 65° delta wing, flat upper surface. Oil-flow pattern on lower surface at $\alpha = 10°$.

Publications of the Aeronautical Research Council

ANNUAL TECHNICAL REPORTS OF THE AERONAUTICAL RESEARCH COUNCIL (BOUND VOLUMES)

1945 Vol.   I. Aero and Hydrodynamics, Aerofoils. £6 10s. (£6 13s. 6d.)
   Vol.   II. Aircraft, Airscrews, Controls. £6 10s. (£6 13s. 6d.)
   Vol. III. Flutter and Vibration, Instruments, Miscellaneous, Parachutes, Plates and Panels, Propulsion.
                                                           £6 10s. (£6 13s. 6d.)
   Vol.   IV. Stability, Structures, Wind Tunnels, Wind Tunnel Technique. £6 10s. (£6 13s. 3d.)

1946 Vol.   I. Accidents, Aerodynamics, Aerofoils and Hydrofoils. £8 8s. (£8 11s. 9d.)
   Vol.   II. Airscrews, Cabin Cooling, Chemical Hazards, Controls, Flames, Flutter, Helicopters, Instruments and Instrumentation, Interference, Jets, Miscellaneous, Parachutes. £8 8s. (£8 11s. 3d.)
   Vol. III. Performance, Propulsion, Seaplanes, Stability, Structures, Wind Tunnels. £8 8s. (£8 11s. 6d.)

1947 Vol.   I. Aerodynamics, Aerofoils, Aircraft. £8 8s. (£8 11s. 9d.)
   Vol.   II. Airscrews and Rotors, Controls, Flutter, Materials, Miscellaneous, Parachutes, Propulsion, Seaplanes, Stability, Structures, Take-off and Landing. £8 8s. (£8 11s. 9d.)

1948 Vol.   I. Aerodynamics, Aerofoils, Aircraft, Airscrews, Controls, Flutter and Vibration, Helicopters, Instruments, Propulsion, Seaplane, Stability, Structures, Wind Tunnels. £6 10s. (£6 13s. 3d.)
   Vol.   II. Aerodynamics, Aerofoils, Aircraft, Airscrews, Controls, Flutter and Vibration, Helicopters, Instruments, Propulsion, Seaplane, Stability, Structures, Wind Tunnels. £5 10s. (£5 13s. 3d.)

1949 Vol.   I. Aerodynamics, Aerofoils. £5 10s. (£5 13s. 3d.)
   Vol.   II. Aircraft, Controls, Flutter and Vibration, Helicopters, Instruments, Materials, Seaplanes, Structures, Wind Tunnels. £5 10s. (£5 13s.)

1950 Vol.   I. Aerodynamics, Aerofoils, Aircraft. £5 12s. 6d. (£5 16s.)
   Vol.   II. Apparatus, Flutter and Vibration, Meteorology, Panels, Performance, Rotorcraft, Seaplanes.
                                       £4 (£4 3s.)
   Vol. III. Stability and Control, Structures, Thermodynamics, Visual Aids, Wind Tunnels. £4 (£4 2s. 9d.)

1951 Vol.   I. Aerodynamics, Aerofoils. £6 10s. (£6 13s. 3d.)
   Vol.   II. Compressors and Turbines, Flutter, Instruments, Mathematics, Ropes, Rotorcraft, Stability and Control, Structures, Wind Tunnels. £5 10s. (£5 13s. 3d.)

1952 Vol.   I. Aerodynamics, Aerofoils. £8 8s. (£8 11s. 3d.)
   Vol.   II. Aircraft, Bodies, Compressors, Controls, Equipment, Flutter and Oscillation, Rotorcraft, Seaplanes, Structures. £5 10s. (£5 13s.)

1953 Vol.   I. Aerodynamics, Aerofoils and Wings, Aircraft, Compressors and Turbines, Controls. £6 (£6 3s. 3d.)
   Vol.   II. Flutter and Oscillation, Gusts, Helicopters, Performance, Seaplanes, Stability, Structures, Thermodynamics, Turbulence. £5 5s. (£5 8s. 3d.)

1954   Aero and Hydrodynamics, Aerofoils, Arrester gear, Compressors and Turbines, Flutter, Materials, Performance, Rotorcraft, Stability and Control, Structures. £7 7s. (£7 10s. 6d.)

Special Volumes

   Vol.   I. Aero and Hydrodynamics, Aerofoils, Controls, Flutter, Kites, Parachutes, Performance, Propulsion, Stability. £6 6s. (£6 9s.)
   Vol.   II. Aero and Hydrodynamics, Aerofoils, Airscrews, Controls, Flutter, Materials, Miscellaneous, Parachutes, Propulsion, Stability, Structures. £7 7s. (£7 10s.)
   Vol. III. Aero and Hydrodynamics, Aerofoils, Airscrews, Controls, Flutter, Kites, Miscellaneous, Parachutes, Propulsion, Seaplanes, Stability, Structures, Test Equipment. £9 9s. (£9 12s. 9d.)

Reviews of the Aeronautical Research Council

     1949-54   5s. (5s. 5d.)

Index to all Reports and Memoranda published in the Annual Technical Reports

     1909-1947   R. & M. 2600 (out of print)

Indexes to the Reports and Memoranda of the Aeronautical Research Council

Between Nos. 2451-2549: R. & M. No. 2550 2s. 6d. (2s. 9d.); Between Nos. 2651-2749: R. & M. No. 2750 2s. 6d. (2s. 9d.); Between Nos. 2751-2849: R. & M. No. 2850 2s. 6d. (2s. 9d.); Between Nos. 2851-2949: R. & M. No. 2950 3s. (3s. 3d.); Between Nos. 2951-3049: R. & M. No. 3050 3s. 6d. (3s. 9d.); Between Nos. 3051-3149: R. & M. No. 3150 3s. 6d. (3s. 9d.); Between Nos. 3151-3249: R. & M. No. 3250 3s. 6d. (3s. 9d.); Between Nos. 3251-3349: R. & M. No. 3350 3s. 6d. (3s. 10d.)

Prices in brackets include postage

Government publications can be purchased over the counter or by post from the Government Bookshops in London, Edinburgh, Cardiff, Belfast, Manchester, Birmingham and Bristol, or through any bookseller